Author Manuscript

Author Manuscript

Author Manuscript

Author Manuscript

HHS Public Access

Author manuscript

Nat Med. Author manuscript; available in PMC 2022 November 01.

Published in final edited form as:

Nat Med. 2022 May ; 28(5): 1050–1062. doi:10.1038/s41591-022-01724-3.

Immunopathological signatures in multisystem inflammatory syndrome in children and pediatric COVID-19

A full list of authors and affiliations appears at the end of the article.

Abstract

Pediatric COVID-19 (pCOVID-19) is rarely severe, however a minority of SARS-CoV-2-infected children may develop multisystem inflammatory syndrome in children (MIS-C), with significant morbidity. In this longitudinal multi-institutional study, we applied multi-omics (analysis of soluble biomarkers, proteomics, single-cell gene expression profile and immune repertoire) to profile children with COVID-19 (n=110) and MIS-C (n=76), along with pediatric healthy controls (pHC; n=76). pCOVID-19 was characterized by robust type I IFN responses, whereas prominent type II IFN- and NF-κB dependent signatures, matrisome activation, and increased levels of circulating Spike protein were detected in MIS-C, with no correlation with SARS-CoV-2 PCR status around the time of admission. Transient expansion of *TRBV11–2* T-cell clonotypes in MIS-C was associated with signatures of inflammation and T-cell activation. The association of

[#]Corresponding Author: Luigi D. Notarangelo, M.D., Laboratory of Clinical Immunology and Microbiology, National Institute of Allergy and Infectious Diseases, National Institutes of Health, Building 10, room 5-3950, 10 Center Drive – MSC, Bethesda, MD 20892, Tel: (301)-761-7550, luigi.notarangelo2@nih.gov.

[*]Equally contributing co-first authors

[†]List of participants and their affiliations appear at the end of the paper

Author Contributions

KS, RC, SV, CL performed experiments, analyzed data, wrote and reviewed the manuscript and prepared figures and tables; OMD, CO, SA, FB, AADJ, LBR, ES, FP, DLF, DG, VO, JC, BAS, TH, MA, SH, DBK, MSL, and RG-M performed experiments, analyzed results and contributed to the writing of the manuscript; KD, YZ, MB, TK, and JJD coordinated collection, processing and cataloguing of samples; SMH supervised analysis of autoantibodies; JL analyzed HLA typing; ALS and CLD performed DNA extraction and genomic sequencing allowing resolution of HLA alleles; IMK and TMS performed high-throughput sequencing of TCR and BCR repertoire; PDB and JIC performed serology studies; AC analyzed autoantibody data; MSV analyzed data; GAMS, KB, MAS and MM reviewed clinical metadata; ER-J, CV, MCP, AL, DM, GLM, FL, UR, VD, ALV, AG, EME, LI, AS, AB, SM, DG and MT consented patients, provided biological specimens and clinical metadata; HCS coordinated with LDN collection and processing of the samples and the research project overall; JST supervised CITE-Seq experiments and critically reviewed the draft of the manuscript; LDN coordinated and supervised the research project, wrote and revised the manuscript and prepared figures and tables.

Competing Interests Statement

TH and SH are employees and shareholders of CDI Laboratories. MA is a consultant for CDI Laboratories and the owner of Biomedical Hosting, LLC. TMS and IMK declare employment and equity ownership with Adaptive Biotechnologies. BAS is a former SomaLogic, Inc. (Boulder, CO, USA) employee and a company shareholder. The remaining authors declare no competing interests.

Group Authors

Members of the NIAID Immune Response to COVID Group:

Jason Barnett[29], Xi Cheng[29], Krishnaveni Kaladi[29], Vasudev Kuram[4], Joseph Mackey[30], Neha M. Bansal[28], Andrew J. Martins[28], Boaz Palterer[1], Helen Matthews[25], Uma Mudunuri[4], Marshall Nambiar[29], Andrew J. Oler[29], Andre Rastegar[1], Smilee Samuel[29], Conrad Shyu[29], Varsha Waingankar[29], Sarah Weber[25], Sandhya Xirasagar[29]

[29] Bioinformatics and Computational Biosciences Branch, Office of Cyber Infrastructure and Computational Biology, National Institute of Allergy and Infectious Diseases, National Institute of Allergy and Infectious Diseases, Bethesda, MD 20982, USA

[30] Operations Engineering Branch, Office of Cyber Infrastructure and Computational Biology, National Institute of Allergy and Infectious Diseases, NIH, Bethesda, MD 20982, USA

Members of the Chile MIS-C Group:

Yazmin Espinosa[16], Camila Astudillo[16], Cecilia Piñera[31], Ricardo González[31]

[31]Hospital Exequiel González Cortés, San Miguel, Chile

Members of the Pavia Pediatric COVID-19 Group:

Maria De Filippo[2], Martina Votto[2], Lorenza Montagna[2]

Author Manuscript Author Manuscript Author Manuscript Author Manuscript

MIS-C with the combination of HLA A*02, B*35, C*04 alleles suggests genetic susceptibility. MIS-C B cells showed higher mutation load compared to pCOVID-19 and pHC. These results identify distinct immunopathological signatures in pCOVID-19 and MIS-C, which may help better define the pathophysiology of these disorders and guide therapy.

Introduction

Following infection with severe acute respiratory syndrome coronavirus 2 (SARS-CoV-2), most children develop mild and self-limiting symptoms of coronavirus disease 2019 (COVID-19)[1], although severe cases and fatal outcomes have been also reported[2]. However, approximately 3–4 weeks after exposure to SARS-CoV-2, some children develop a hyperinflammatory response resembling Kawasaki Disease (KD) and toxic shock syndrome that has been termed multisystem inflammatory syndrome in children (MIS-C)[3–5].

The mechanisms underlying the different picture of pediatric COVID-19 (pCOVID-19) and MIS-C remain ill-defined. Older age, male sex, obesity, co-existing comorbidities, genetic defects of Toll-like receptor (TLR)3- and TLR7-dependent type I interferon (IFN) pathways, and neutralizing autoantibodies against type I IFNs are associated with more severe clinical outcomes in adults with COVID-19 (aCOVID-19)[6–9]. More limited information is available on the immune response to acute SARS-CoV-2 infection in children[10]. Elevated serum levels of several inflammatory biomarkers, an expansion of T cell clonotypes expressing the T-cell receptor (TCR) *TRBV11–2* gene (possibly in response to a SARS-CoV-2 superantigen), and presence of autoantibodies directed against several self-antigens have been reported in MIS-C[11–15].

The magnitude of the inflammatory response in MIS-C correlates with disease severity[13,16], and use of glucocorticoids and intravenous immunoglobulins (IVIG), improves clinical outcome[17], whereas limited data are available on the efficacy of biologics, such as IL-1 receptor (IL-1R)- and Tumor Necrosis Factor-α (TNF-α)-antagonists and tocilizumab[18,19]. Nevertheless, the temporal trajectory of inflammatory markers in response to treatment during the course of the disease has not been elucidated. In this study, we used a multi-omics approach (with analysis of soluble biomarkers, proteomics, single-cell gene expression profile, T- and B-cell receptor repertoires and autoantibodies) to comparatively assess longitudinal changes of innate and adaptive immune responses of pCOVID-19 and MIS-C, and identified distinct signatures associated with pCOVID-19 and MIS-C that may help define the pathophysiology of these disorders and guide treatment.

Results

Characteristics of the study cohorts

We included a total of 186 pediatric patients (110 with pCOVID-19 and 76 with MIS-C) and 76 pediatric healthy controls (pHC). The demographic, clinical and laboratory characteristics of patients and pHC are reported in Table 1, and the number of patients analyzed with various assays is outlined in Figure 1.

Author Manuscript Author Manuscript Author Manuscript Author Manuscript

Soluble biomarkers in the early phase of pCOVID-19 and MIS-C

To explore early immune and inflammatory responses, we measured levels of 50 soluble biomarkers in serum or plasma obtained from 57 children with pCOVID-19 within 7 days since onset of symptoms [median, 2 days; interquartile range (IQR), 1–3 days], and in 48 children with MIS-C within 7 days from hospitalization ("MIS-C Early"; median, 2 days; IQR, 1–4 days). Soluble biomarkers were also measured in 60 MIS-C patients >7 days after admission ("MIS-C Late"; median, 14 days; IQR, 10.25–31 days) and in 53 pHC. Distinctive signatures characterized pCOVID-19 and MIS-C. Higher levels of IFN-α2a were detected in pCOVID-19 (Figure 2a), especially in children with mild disease (Extended Data Figure 1a). High levels of IFN-α2a in pCOVID-19 were associated with a higher type I IFN score, as determined by a NanoString assay capturing expression of 28 type I IFN-stimulated genes in both myeloid and lymphoid cells[20] (Figure 2b). In addition, pCOVID-19 was also characterized by low levels of IL-33, an epithelial and endothelial cell alarmin, and by increased levels of some inflammatory biomarkers, whose levels rapidly declined over time (Figure 2a and Extended Data Figure 2a–b). However, NanoString analysis of the expression of 15 type II IFN-dependent and of 11 nuclear factor (NF)-κB-responsive genes did not reveal differences between pCOVID-19 and pHC (Figure 2c).

To investigate whether age plays an important role in modulating inflammatory responses (including attenuated inflammation in pCOVID-19 compared to aCOVID-19), we compared levels of soluble biomarkers measured in moderate forms of pCOVID-19 (n=9) and aCOVID-19 (n=26)[21], as well as in pHC (n=53) and adult healthy controls (aHC, n=45). For most biomarkers (38/50), blood levels differed between pHC and aHC (Extended Data Table 1), indicating that age plays an important role in setting baseline immune status. Adjustment for these baseline differences is necessary when interpreting the influence of COVID-19 (Extended Data Figure 1b–d).

Analysis of MIS-C samples obtained within 7 days of hospitalization in 48 patients demonstrated a significant increase in biomarkers related to type II IFN signaling (IFN-γ, CXCL9, CXCL10), macrophage activation (IL-6, sTNFRI, IL-10, sCD25, IL-17, TNF-α, sCD163, CCL2, CCL3, CCL4, ferritin, IL-15), endothelial injury and activation (VEGF, sVCAM-1/sCD106, sE-Selectin/sCD62E), neutrophil activation (MPO, lactoferrin), matrisome-related inflammation (MMP-9, sST2/sIL-33R, CX3CL1) and septic shock (LBP), and low levels of CCL22 (Figure 2a and Extended Data Figure 2b). The SARS-CoV-2 PCR status around the time of admission had no significant impact on the clinical presentation and on the levels of soluble biomarkers (Supplementary Table 1 and Supplementary Figure 1). For most biomarkers, levels tended to decrease at later time points (MIS-C Late) during hospitalization (Figure 2a and Extended Data Figure 2b), concurrent with clinical improvement. Consistent with this broad inflammatory signature, NanoString analysis of 15-gene type II IFN-dependent and of 11 nuclear factor (NF)-κB-responsive genes revealed significantly higher scores in paired samples obtained from MIS-C patients at earlier *versus* later time points during hospitalization (Figure 2c), and a similar pattern was observed also for type I IFN score (Figure 2b).

Feature importance analysis based on random forest classification (that also included age, sex and ethnicity) identified low levels of IL-33 and increased levels of IL-6, TNF-α,

Author Manuscript Author Manuscript Author Manuscript Author Manuscript

ferritin, CCL2, MPO, IL-15, IFN-α2a, soluble VCAM-1 (sVCAM-1), and IL-10 as the most important parameters distinguishing pCOVID-19 from pHC (Figure 2d). Using the same approach, elevated levels of several inflammatory biomarkers, and low levels of CCL22 emerged as the most important parameters distinguishing MIS-C Early from pHC (Figure 2e). Furthermore, random forest classification identified molecules involved in matrisome (sST2/sIL-33R), intestinal inflammation and myocardial damage (Reg3A) and T cell homeostasis (CCL22) as the most important factors distinguishing MIS-C from pCOVID-19 (Figure 2f). Multivariate regression analysis identified IL-33 as the only biomarker whose levels were significantly different in pCOVID-19 vs. pHC, whereas CCL3 and IL-15 distinguished MIS-C from pHC and pCOVID-19, respectively, with a role also for CCL22 in both cases (Extended Data Table 2). The prominent inflammatory signature of MIS-C was associated with significantly elevated levels of soluble Spike protein (Figure 2g). Of note, among 15 patients in whom Spike protein levels >40 pg/mL were detected within 7 days after admission, only 2 tested positive for SARS-CoV-2 mRNA in nasopharyngeal swabs. Finally, anti-Spike (anti-S) and anti-Nucleocapsid (anti-N) antibody levels were significantly higher in MIS-C than in pCOVID-19 (Extended Data Figure 2c), consistent with the limited time interval between onset of symptoms and sample collection in the pCOVID-19 group.

Proteomic analysis of immunopathological signatures

To gain additional insights into the inflammatory signature of MIS-C and pCOVID-19, we performed proteomic profiling of a subgroup of subjects using *SOMAscan®22*. In 10 pCOVID-19 patients, we observed a limited number of up- and down-regulated proteins (26 and 25, respectively) relative to 4 pHC, including increased levels of myeloid activation-associated proteins (MPO, IL18R1, TNFAIP6, ACP5), and SIGLEC7, an inhibitor of natural killer (NK) cell pyroptosis and inflammasome activation[23] (Figure 3a–b). Gene set enrichment analysis (GSEA) revealed molecular signatures of immune activation, compatible with active SARS-CoV-2 viral infection (Figure 3a).

A marked inflammatory profile was observed in MIS-C patients, with a high number of significantly increased (n=242) and decreased proteins (n=158) compared to pHC (Figure 3c–d). MIS-C patients had increased levels of several inflammatory biomarkers [serum amyloid A (SSA1), CRP, ferritin, CXCL10, sST2/sIL-33R, CXCL9] and of B natriuretic peptide (NPPB.1), the latter consistent with cardiac involvement in MIS-C. GSEA showed hyperactivation of the matrisome-associated response. Overall, the inflammatory activation observed in MIS-C appeared to be higher and qualitatively different from pCOVID-19 (Figure 3e–f).

Longitudinal evolution of blood biomarkers in MIS-C

We hypothesized that the differences in soluble biomarker levels detected at early and later time points during the course of MIS-C (Figure 2a and Extended Data Figure 2b) could be due to early intervention with systemic glucocorticoids and IVIG[17]. However, how these interventions modulate the inflammatory response has not been elucidated. The timeline of initiation of therapeutic intervention with various classes of drugs and blood sampling compared to day of admission in MIS-C patients is reported in Extended Data Figure 3. We identified 12 patients for whom biomarker levels were measured both prior

Author Manuscript Author Manuscript Author Manuscript Author Manuscript

to (median, 0 day; IQR −1 to 0 days) and after (median, +5 days, IQR +4 to +7.5 days) glucocorticoid administration. Two of these patients had previously received IVIG, and eight additional patients received IVIG in the interval. Biomarkers associated with Type II IFN response (IFN-γ, CXCL9), T cell activation (sCD25), cell adhesion (sE-Selectin/sCD62E) and monocyte/macrophage activation (sTNFRII, M-CSF, ferritin, IL-6) decreased following treatment (Extended Data Figure 4a). To investigate how rapidly treatment with glucocorticoids and/or IVIG may impact on the inflammatory phenotype, we re-analyzed the MIS-C Early cohort, segregating patients into two groups: those whose blood samples were drawn prior (n=12) or after (n=36) therapeutic intervention. A significant difference of blood levels between untreated and pre-treated MIS-C Early patients was observed for four biomarkers [lymphotoxin-α (LT-α), lactoferrin, IL-12p70 and IL-5], and a similar trend was present for several other proteins (Extended Data Figure 4b). Furthermore, treatment prior to blood sampling was not among the top 10 most important variables when introduced in the random forest regression analysis comparing MIS-C Early *versus* pHC (Extended Data Figure 4c). Altogether, these data indicate that treatment did not entirely obscure the hyperinflammatory phenotype that characterizes MIS-C early in the course of the disease. However, longitudinal analysis during the entire course of hospitalization revealed a negative correlation between length of hospitalization and levels of most soluble biomarkers in patients who had received glucocorticoids, irrespective of whether IVIG was administered or not (Supplementary Figure 2a–b). Random forest regression analysis identified several biomarkers that were of higher median predictive importance in patients who received glucocorticoids (Figure 3g); concurrent use of IVIG had a more specific effect on IL-1R antagonist (IL-1Ra), MPO, sIL-2Rα, sTNFRI, LBP, sICAM-1, CCL3 and sCD163.

Multimodal single cell profiling of MIS-C and pCOVID-19

To better understand and compare the cell type specific gene expression profile of MIS-C and pCOVID-19, we performed single-cell CITE-seq[24,25] in peripheral blood mononuclear cells (PBMC) from 7 MIS-C, 8 pCOVID-19 and 7 age- and sex-matched pHC. Two longitudinal samples were available for 3 MIS-C patients. We also performed CITE-seq profiling on sorted non-naïve T and B cells to enhance TCR and BCR clonality analysis. Unsupervised clustering identified 24 annotated coarser level cell populations (Figure 4a). Integrating the CITE-seq data with previously published aCOVID-19 datasets[25] yielded largely concordant cell clusters (Extended Data Figure 5a). The frequency of non-classical monocytes was reduced in MIS-C patients; a similar pattern was observed in aCOVID-19, and especially in those with more severe disease[25] [Disease Severity Matrix (DSM)_high in Extended Data Figure 5b]. Reduced frequencies of plasmacytoid dendritic cells (pDC) were detected in MIS-C, but not in pCOVID-19 compared to pHC. Another characteristic of pCOVID-19 was the increased frequency of CD8+ memory T cells, which was also noted in adults with less severe disease (DSM_low in Extended Data Figure 5b).

We next systemically assessed cell type specific transcriptional changes among pHC, pCOVID-19, and MIS-C using the cell clusters derived from surface proteins (Figure 4b and Extended Data Figure 5c). Strong T and B cell activation signatures and increased antigen presentation in both innate and adaptive cell populations were observed in both pCOVID-19 and MIS-C groups compared to pHC (Figure 4b and Extended Data

Author Manuscript Author Manuscript Author Manuscript Author Manuscript

Figure 5c). Consistent with a recent report[13], we observed enrichment of the gene set "KEGG_Natural_Killer_cell_mediated_cytotoxicity" in CD16^{hi} NK cells from MIS-C, but not from pCOVID-19 patients (Figure 4b and Extended Data Figure 5c).

Type I IFN signatures (including gene signatures induced by live viral challenge or vaccination[26,27]) were strongly elevated in almost all immune cell subsets in pCOVID-19 but only in a few MIS-C adaptive cell populations and pDCs (Figure 4b and Extended Data Figure 5c); MIS-C exhibited broadly lower type I IFN signatures across cell types compared to pCOVID-19 (Figure 4b). Consistent with our prior CITE-seq analysis in adults[25], time effect analysis hinted that the type I IFN signature in pCOVID-19 decreased over time in most cell types (Figures 4c, top), although we caution that the number of longitudinal samples was small.

Although classical monocyte cell frequencies were similar, the mRNA based uniform manifold approximation and projection (UMAP) visualization of monocytes showed separation among pHC, pCOVID-19, and MIS-C (Extended Data Figure 5d, left panel). Specifically, MIS-C monocytes showed significantly higher levels of CD163 expression and of several S100A family inflammatory genes; the latter were also increased (although to a lesser degree) in pCOVID-19 monocytes compared to pHC (Extended Data Figure 5d, middle and right). However, classical monocytes from MIS-C patients showed repressed inflammatory signatures (HALLMARK_TNFα_via_NFκB signaling and HALLMARK_inflammatory response pathways/gene sets) compared to both pCOVID-19 and pHC (Figures 4b, d and e). Intriguingly, the lymphocytes (CD4+ and CD8+ T cells and NK cells) and DC populations tended to have lower inflammatory signatures instead in pCOVID-19 than in both MIS-C and pHC (Figures 4b, d and e, and Extended Data Figure 5c). This repressed inflammatory gene signatures in non-monocyte populations in pCOVID-19 could point to differences in the systemic immune responses in children compared to adults, as also recently reported by others[28].

To validate these observations, we interrogated an independent published cohort with single-cell data[13], and observed similarly strong signatures of T and B cells, NK and CD8+ T cell cytotoxicity, and enhanced type I IFN response (mainly seen in T and B cell populations) in MIS-C patients (Supplementary Figure 3a). The repressed inflammatory signatures of monocytes were also seen in this validation cohort with overlapping leading-edge genes driving these repressed signatures (Supplementary Figure 3a–b). We next visually assessed these leading-edge genes from the MIS-C *versus* pCOVID-19 comparison in our cohort by plotting the cell type specific expression heatmaps of these genes using data from the validation cohort[13]. This revealed that these genes indeed tend to have lower expression in classical monocytes in MIS-C compared to pHC, although this trend appeared less significant in memory CD4+ T cells (Supplementary Figure 3b).

TRBV11–2 usage over time in MIS-C CD4+ T cells

Bulk high-throughput sequencing of TCRβ (TRB) repertoire was performed to analyze the breadth of the SARS-CoV-2 specific TCR repertoire, representing the fraction of TRB clonotypes that are SARS-CoV-2 specific in each repertoire. A modest increase in the

Author Manuscript Author Manuscript Author Manuscript Author Manuscript

breadth of SARS-CoV-2 specific clonotypes was observed in pCOVID-19 and MIS-C compared to pHC (Extended Data Figure 6a).

Analysis of *TRB* Variable (*TRBV*) gene usage revealed markedly increased frequency of *TRBV11–2* clonotypes in MIS-C (Figure 5a), confirming previous reports[13–15,29,30]. Interestingly, such increased frequency of *TRBV11–2* clonotypes was restricted to MIS-C samples that were collected soon after hospitalization, whereas a rapid decline in the proportion of *TRBV11–2* clonotypes was observed thereafter (Figure 5b), as also reported by others[15]. Both the increased *TRBV11–2* usage and the progressive decline in the frequency of *TRBV11–2* clonotypes were confirmed in CITE-seq profiling of CD4+ T cells (Figure 5c) of MIS-C patients. Computational analysis revealed enrichment of unique SARS-CoV-2 specific CDR3 clonotypes among *TRBV11–2* positive clonotypes in all groups (MIS-C, pCOVID-19 and pHC); however, such enrichment was significantly lower in MIS-C patients compared to pCOVID-19 and pHC (Extended Data Figure 6b). Moreover, *TRBV11–2* clonotypes of MIS-C patients were characterized by a diverse usage of associated *TRBJ* genes (Supplementary Figure 4a) and a broad distribution of CDR3 length (Supplementary Figure 4b), arguing against oligoclonal expansions.

The frequency of *TRBV11–2* clonotypes in MIS-C positively correlated with levels of several inflammatory biomarkers (Extended Data Figure 6c), consistent with previous observations[14]. Single cell CITE-seq gene expression analysis showed slightly higher average expression of genes associated with T-cell activation (*HCST* and *DUSP2*) and effector function (*GZMK, PRF1, GZMA* and *IL32*), immune cell synapse and adhesion formation (*PSMB1, HAVCR2, SIRPG, CTLA4, RAC2, MSN, ITGB2,* and *SELL*), and IL-2 and IL-15 signaling response pathways (*SIRPG*, *IL2RB*, and *IL2RG*) in *TRBV11–2* CD4+ T cell clones compared with other CD4+ MIS-C T cells (Extended Data Figure 6d). Differential expression analysis on the cell surface markers [CITE-seq antibody data (ADT)] revealed higher expression of T cell co-stimulatory molecules CD28 and CD150 (SLAM) (Extended Data Figure 6e). Furthermore, the transcriptional signature of *TRBV11–2* CD4+ T cells was characterized by increased expression of genes involved in apoptosis and lymphocyte activation (Extended Data Figure 6f and Supplementary Table 2).

Interestingly, time elapsed from the first use of glucocorticoids negatively correlated with the frequency of *TRBV11–2* clonotypes (Extended Data Figure 6g) and was predictive of reduced *TRBV11–2* gene usage over time (Extended Data Figure 6h). This suggests that the use of glucocorticoids might have contributed to the apoptosis transcriptional signatures we saw in the single cell analysis above (Extended Data Figure 6f), even though this could also reflect the contraction of CD4+ T cell subsets during the resolution of disease[31–33].

It has been previously shown that MIS-C patients with a severe clinical phenotype and expansion of *TRBV11–2* share the combination of HLA class I alleles A*02, B*35 and C*04, indicating a possible contribution of HLA-mediated restriction in the process of *TRBV11–2* expansion[29]. To determine whether a similar association was found in our patient cohort and avoid confounding factors due to different frequencies of HLA alleles in different ethnic groups, we analyzed a sub-cohort of Italian patients only (MIS-C, n=9; pCOVID-19, n=64; pHC, n=44) which we further restricted by selecting subjects of

Author Manuscript Author Manuscript Author Manuscript Author Manuscript

predicted European ancestry (MIS-C, n=7; pCOVID-19, n= 45; pHC, n= 35). The A*02, B*35, C*04 allele combination was present in 5 of the 7 MIS-C, 2/35 pHC and in none of the 45 pCOVID-19, reaching statistical significance (Extended Data Table 3). Of note, the combination of HLA A*02, B*35, C*04 allele was not associated with severity of the MIS-C phenotype, as it was found in 4 patients with moderate and one child with severe disease.

B-cell activation and repertoire in MIS-C

Previous studies have documented B cell abnormalities in severe aCOVID-19 and in MIS-C, with increased number of IgD^{-} $CD27^{-}$ $CD11c^{+}$ cells in the former[34] and of plasmablasts in both conditions[34,35], along with increased frequency of *IGHV4–34* and *IGHV4–39* clonotypes[14,34], and presence of autoantibodies against a variety of self-antigens[12–14]. High-throughput sequencing of the *IGH* repertoire in 13 pHC, 15 pCOVID-19, and 19 MIS-C did not reveal major differences in the usage of *IGHV* genes (Extended Data Figure 7a–b), but demonstrated an increased rate of somatic hypermutation (SHM) among MIS-C *IGHV* clonotypes (Extended Data Figure 7c). CITE-Seq analysis revealed a significantly increased frequency of SHM in plasmablasts in MIS-C compared to pCOVID-19 (Figure 5d), and a similar trend was observed in memory B cells (Extended Data Figure 7d). Several surface markers associated with B cell activation correlated with mutation frequencies within memory B cells (lower IgD, CD305, and IgM; and, higher CD27, CD95, CD71, and CD99; Extended Data Figure 7e) and plasmablasts (CD95, CD99 and HLA-DR; Extended Data Figure 7f).

To investigate the presence of autoantibodies, we used the human proteomic (HuProt™) assay comparing 10 MIS-C samples (4 with and 6 without prior IVIG treatment) to 5 pCOVID-19. We detected several autoantibodies in MIS-C, including previously reported TROVE2/Ro60 and ATP4A[14] (Figure 5e). However, positivity was mostly evident in MIS-C samples drawn after IVIG administration, suggesting that IVIG may represent an important confounding factor in the evaluation of the presence of autoantibody in MIS-C. Pre-existing neutralizing autoantibodies targeting IFN-α and/or IFN-ω are frequently detected in critical aCOVID-19[9]. To investigate whether such autoantibodies are also present in children, we screened serum from pHC (n=53), pCOVID-19 (n=70), and MIS-C (n=40). Borderline levels of positive immunoreactivity against IFN-α and/or IFN-ω were detected in a few MIS-C and pCOVID-19 patients, and no neutralizing activity was detected (Supplementary Figure 5).

Discussion

Defining the pathophysiology underlying distinct SARS-CoV-2 related diseases in children represents an important medical need. Type I IFN-dependent responses play a critical role in controlling replication of respiratory tract viruses early after infection[36]. Defective type I-IFN responses have been demonstrated in severe aCOVID-19[37,38]. Our observations of intact frequencies of pDCs in pCOVID-19, associated with robustly elevated IFN-α2a levels and increased expression of type I IFN-dependent genes in peripheral blood samples collected within 7 days from onset of symptoms, contrast with findings in aCOVID-19,

Author Manuscript Author Manuscript Author Manuscript Author Manuscript

and are consistent with the demonstration that pre-activated antiviral innate immunity in the upper airways controls early SARS-CoV-2 infection in children[28,39].

We identified reduced induction of systemic inflammatory responses as another important feature distinguishing pCOVID-19 *versus* aCOVID-19[21,25], as shown by lower levels of inflammatory biomarkers and decreased transcriptional inflammatory signatures of lymphocyte and DC populations in the former.

The identification of decreased IL-33 levels in pCOVID-19 represents a finding which needs validation in other cohorts. IL-33 is a member of the IL-1 cytokine family and is released mainly by epithelial cells upon infection, cell damage or exposure to allergens[40,41]. High IL-33 levels are increased in children with severe viral and bacterial infections[42–45]. The low IL-33 levels detected in pCOVID-19 may be indicative of modest respiratory epithelium cell damage, whereas high levels of IL-33 were previously demonstrated by our group in critical, but not moderate aCOVID-19[21].

Analysis of soluble biomarker levels in MIS-C revealed low levels of CCL22, a homeostatic chemokine that promotes regulatory T cell migration and function[46]. By dampening regulatory T cell responses, low CCL22 levels in MIS-C may favor uncontrolled inflammation. Importantly, both IL-33 and CCL22 are involved in Th2 responses[47,48], and both are negatively regulated by IFN-γ[49,50]. Along with increased levels of IFN-γ in MIS-C (and to a lesser extent in pCOVID-19), these observations indicate that pCOVID-19 and MIS-C are characterized by prominent Th1 and suppressed Th2 responses.

Consistent with previous observations[11–13,16], we have shown that MIS-C patients had elevated levels of soluble biomarkers associated with recruitment and activation of monocytes and neutrophils, vascular endothelium injury, matrisome activation, gastrointestinal and cardiac involvement, and septic shock. Activation of matrisome which encompasses proteins associated with the extracellular matrix including the endothelium[51], and increased levels of biomarkers indicative of endothelial cell damage in MIS-C, mirror what is observed in various vasculitides, including KD[52].

In addition, CITE-Seq analysis revealed a MIS-C monocyte signature characterized by increased expression of several members of the S100A family of alarmins and of the scavenger receptor CD163. However, in comparison to pCOVID-19, MIS-C monocytes had lower type I IFN and NF-κB/inflammatory signatures and repressed antigen presentation genes, which were phenotypically similar to the MS1 monocyte cell state reported in severe aCOVID-19 and in bacterial sepsis[53,54]. These reduced inflammatory signatures of monocytes in MIS-C may have been contributed by the routine administration of glucocorticoids and IVIG early in the course of the disease.

In our study, elevated levels of soluble Spike protein were detected in 15/21 MIS-C patients. A previous study had correlated elevated Spike protein levels in MIS-C to persistence of SARS-CoV-2 in the gastrointestinal tract[55]. While we did not investigate the presence of SARS-CoV-2 mRNA in stool samples, only 2 of these 15 MIS-C patients had a positive PCR on nasopharyngeal swab within 7 days after admission, indicating that elevated Spike protein levels were not due to persistent respiratory tract infection.

Author Manuscript Author Manuscript Author Manuscript Author Manuscript

Analysis of the T- and B-cell repertoires revealed other important features of pCOVID-19 and MIS-C. The modest increase in the breadth of SARS-CoV-2 specific CDR3 clonotypes in children with pCOVID-19 and MIS-C compared to pHC is consistent with previous studies demonstrating that younger individuals have pre-existing CD4+ T cells to human endemic β-coronaviruses that are cross-reactive to SARS-CoV-2 Spike protein[56,57] and that may help contain virus replication, limiting the development of a larger pool of newly generated SARS-CoV-2 specific T cells in infected children.

We have confirmed previous observations demonstrating an expansion of *TRBV11–2+* polyclonal T cells in MIS-C, possibly driven by a superantigen-like motif within the C-terminal region of the Spike S1 subunit[15,29,30,58]. *TRBV11*-2 CD4+ T cells expressed high levels of CD150 and CD28 on their surface, and their transcriptional profile was characterized by expression of genes involved in cell adhesion, activation and of the mitochondrial pathway of apoptosis. Together, these results suggest that *TRBV11–2* expressing T cells represent a cell population poised to respond to activating signals and undergo apoptosis. The proportion of *TRBV11–2* clonotypes positively correlated with levels of various inflammatory biomarkers, and both the frequency of *TRBV11–2* clonotypes and levels of most of these biomarkers decreased within 1–2 weeks after use of glucocorticoids. We postulate that the rapid decrease of *TRBV11–2* clonotypes was contributed by the use of glucocorticoids, that are known to mediate apoptosis of activated T cells, predominantly through the mitochondrial pathway[59–61].

Importantly, by selecting patients of homogeneous predicted ancestry, we have validated the recent demonstration of the association of MIS-C with the combination of the HLA-A*02, B*35, C*04 alleles[29], arguing for a genetic basis of susceptibility to MIS-C.

Analysis of the B-cell compartment of MIS-C patients demonstrated an increased SHM rate in plasmablasts, correlating with increased expression of several activation markers on the cell surface of both memory B cells and plasmablasts. On the other hand, while autoantibodies have been reportedly detected in MIS-C patients also prior to IVIG administration[11–14], we detected them at higher frequency in samples collected after IVIG administration, indicating that use of IVIG is an important confounding factor. Similar observations have been recently obtained in KD[62].

This study has some limitations. Only a few children with severe pCOVID-19 were investigated, and no cases of acutely ill children with conditions other than COVID-19 were included. The transcriptional signature of PBMC was analyzed in a limited number of patients. Nonetheless, we were able to detect early and late signatures of the disease, and the characteristic gene expression profile identified in our cohort correlated with what observed by others[13]. The vast majority of MIS-C patients received treatment with glucocorticoids (alone or in association with IVIG) shortly upon hospitalization, so that it was not possible to define the relative role of therapeutic interventions and natural history of the disease on the dynamic changes of biomarkers analyzed. However, we postulate that timely therapeutic intervention played a critical role in facilitating resolution of inflammatory complications and favorable clinical outcome in all patients included in the study. Too few patients (n=4) received IVIG alone (n=12) or various biologics (n=12) to allow define the specific effects

Author Manuscript Author Manuscript Author Manuscript Author Manuscript

of these treatments. Finally, all blood samples were collected at the time when only the ancestral Wuhan strain, the B1.177 (European lineage) and the 1.1.7 (alpha) variants were circulating at the centers where the patients were enrolled. Therefore, the impact of the delta and omicron variants on innate and adaptive immune responses in children with pCOVID-19 and MIS-C remains to be studied.

Relatively few studies had explored immune responses to SARS-CoV-2 in children, most often in a limited number of subjects. By applying a multi-omics approach to a large cohort of patients, we have demonstrated important differences in the response to acute SARS-CoV-2 infection in children and adults and established that pCOVID-19 and MIS-C have distinctive immunopathological signatures, which may help better characterize the pathophysiology of these disorders and guide optimal treatment.

Methods

Statistics and Reproducibility

This was a natural history study of consecutive cases of patients with pCOVID-19 and MIS-C enrolled at the referring institutions. Informed consent was provided by the parents/guardians, and assent by the minor, when appropriate. No statistical method was used to predetermine sample size. Investigators analyzing biomarker levels were blinded to the characteristic of the patients from whom the blood samples had been obtained.

Study population

The study included 186 pediatric patients (≤ 18 years) with clinically and laboratory confirmed MIS-C (n=76), pCOVID-19 (n=110) and pHC (n=76), whose blood samples were collected between March 30, 2020 and February 8, 2021, upon informed consent and according to protocols approved by local Institutional Review Boards (IRBs): Comité Ético Científico Facultad de Medicina Clínica Alemana Universidad del Desarrollo, Santiago, Chile (protocol 2020–41); Ethics Committee of the Fondazione IRCCS Policlinico San Matteo, Pavia, Italy (protocol 20200037677); Comitato Etico Interaziendale A.O.U. Città della Salute e della Scienza di Torino, Turin, Italy (protocol 00282/2020); Ethics Committee of the University of Naples Federico II, Naples, Italy (protocol 158/20); Comitato Etico Provinciale (protocol NP-4000, Brescia, Italy); University of Milano Bicocca – San Gerardo Hospital, Monza and Ethics Committee of the National Institute of Infectious Diseases “Lazzaro Spallanzani”, Italy (protocol 84/2020); Hadassah Medical Organization Institutional Review Board (IRB), Jerusalem, Israel (protocol HMO-235–20); National Institute of Allergy and Infectious Diseases, National Institutes of Health, Bethesda, MD, USA (protocols NCT04582903, NCT03394053 and NCT03610802).

Clinical datasets from international sites were translated, checked for consistency, transformed to the same scale and units as needed using Python libraries (NumPy, pandas, dateutil) and outliers manually reviewed. The data harmonized across all sites were collected in LabKey® (LabKey Server, Enterprise Edition v21.11.4) where final curation was performed by the clinical research team.

Author Manuscript Author Manuscript Author Manuscript Author Manuscript

The severity of pCOVID-19 was defined as follows: 1) asymptomatic, 2) mild, 3) moderate, 4) severe and 5) critical as per the NIH COVID-19 Treatment Guidelines[63]. The clinical severity was not affected by age, sex, or ethnicity, and there were no fatal outcomes.

MIS-C diagnosis was based on the Center for Disease Control and Prevention (CDC) Health Advisory case definition[5], but only patients with evidence of prior SARS-CoV-2 infection (as determined by positive PCR ± anti-S/anti-N serology) were included. MIS-C patients were divided into moderate (MIS-C-M; n= 52, 68%) and severe (MIS-C-S; n=24, 32%) groups as previously described[13]. All MIS-C patients improved significantly during the hospitalization and were eventually discharged.

For the comparison of pCOVID-19 and aCOVID-19, we used previously published data from our group on biomarkers in aCOVID-19[21], as well as a cohort of healthy adults. For Nanostring and Spike protein levels, pHC samples were obtained from a cohort of healthy children studied by NIAID Translational Autoinflammatory Disease Studies (TADS).

Measurement of soluble biomarkers

Analysis of soluble biomarker levels was performed on plasma or serum obtained from patients with pCOVID-19 (n=110), MIS-C (n=73) and pHC (n=53), including 57 pCOVID-19 and 48 MIS-C patients whose samples were obtained within 7 days since onset of symptoms or hospitalization, respectively. Because of limited available volume, patient samples were analyzed as single determinations. Duplicate determinations of samples from pHC yielded coefficients of variation that were normally <20%. Blood samples were centrifuged, and serum or plasma samples frozen immediately frozen at −85°C prior to analysis. Levels of soluble biomarkers whose data were concordant between both plasma and sera, were measured as previously described[21]. Depending on the nature of the analyte, measurements were obtained using the V-PLEX Human Cytokine 30-Plex Kit (Meso Scale Discovery, Rockville, MD) and analyzed on a MESO QuickPlex SQ 120 reader (Meso Scale Discovery, Rockville, MD), or using a customized, magnetic bead-based, multiplex assay (R&D Systems, Minneapolis, MN) according to the manufacturers' specifications for standards and dilutions, and the magnetic beads were analyzed on Bio-Plex 3D instrumentation (Bio-Rad, Hercules, CS). Standard curves were analyzed using nonlinear curve fitting and unknowns were calculated based on the derived equation. Samples that exceeded the highest standards were reanalyzed at higher dilution dilute until the values fell within the range of the known standards. Two control plasma samples and a control sample spiked with a known quantity of each analyte were analyzed on each plate to assess the inter-plate variation and to determine the effect of the biological matrix on the measurement of each analyte. For most analytes, the control samples had <25% variation from plate to plate, and the recoveries were generally >70%.

For the biomarker values that were below the lower limit of detection (LLOQ) the actual measured concentrations were used or, if unavailable and reported as zeros (for 26 of the 50 biomarkers), values were extrapolated as LLOQ divided by two. The exception was made for the comparison of pCOVID-19 and aCOVID-19, due to the absence of LLOQ for the biomarker measurements in adults. Therefore, only values over zeros were used for that analysis.

Author Manuscript Author Manuscript Author Manuscript Author Manuscript

The univariate analysis of biomarker levels was performed using Mann-Whitney U test (when two groups were compared) or Kruskal-Wallis test (corrected for multiple comparisons) when multiple groups were compared. Biomarkers differing significantly between or among groups were then included in the multivariate model together with age, sex and ethnicity. For the comparison of pCOVID-19 with pHC, allergic conditions (allergic rhinitis, asthma, atopic dermatitis) were also included as a variable in multivariate regression analysis. These analyses were completed with IBM SPSS Statistics v.27 and GraphPad Prism version 9.

For the random forest classification, we used Python v. 3.8.10 and the following libraries: pandas==1.1.2, numpy==1.18.5, scikit-learn==0.23.2, matplotlib==3.3.2. Three models were trained with 53 attributes: (Training set size / Validation set size / Accuracy) pHC vs MIS-C (78 / 20 / 95%), MIS-C *versus* pCOVID-19 (82 / 21 / 100%) and pHC *versus* pCOVID-19 (87 / 22 / 100%). Trained with Python sklearn library's RandomForestClassifier object, using parameters: n_estimator=2000, random_state=42 for data set. Results represent the relative importance of each of the 53 attributes provided by the model attribute RandomForestClassifier.feature_importances_.

Attribute's direction of influence was based on the increase/decrease of its mean values between compared groups. For the comparison of pHC with pCOVID-19, the classification was then repeated after the exclusion of allergic pHC, with similar results.

Spike protein measurement

Patient serum was collected and analyzed for the concentrations of spike protein using COVID-19-Spike-Protein (S1RD) ELISA kit (ab284402, Abcam, Cambridge, MA, USA). Recombinant SARS-CoV-2 S1+S2 ECD (S-ECD) protein (RP01283LQ, ABclonal, MA, USA) was spiked at increasing concentrations into pre-COVID serum from healthy controls and was used as standard for the calculation of the Spike protein concentration. Pre-COVID-19 pediatric (n=7, age 7 to 18) and adult (n=9, age 19 to 63) serum samples were used as controls.

SARS-CoV-2 antibody testing

SARS-CoV-2 anti-S and anti-N antibody testing was performed via luciferase immunoprecipitation systems assay, as previously described[64].

NanoString assay

Total RNA was extracted from whole blood samples collected in PAXgene tubes (Qiagen, Germantown, MD). Gene expression of selected genes was determined by NanoString (NanoString Technologies, Seattle, WA) and a 28-gene type I IFN score and an 11-gene NF-κB score was calculated as previously described[20]. An IFN-γ score was calculated based on 15 IFN-γ-regulated genes[65]. Briefly, the 28-gene type I IFN score is the sum of the z-scores of 28 type I IFN response genes, the 11-gene NF-κB score is the sum of the z-scores of 11 NF-κB target genes and the 15-gene IFN-γ score is the sum of the z-scores of 15 response genes. Individual gene z-scores were calculated using the mean and standard deviation of the NanoString counts from pHC. Nonparametric two-tailed Kruskal-Wallis test

Author Manuscript Author Manuscript Author Manuscript Author Manuscript

(corrected for multiple comparison) was used for group comparisons and p values below 0.05 were considered statistically significant. Statistical analyses were performed using GraphPad Prism version 8.00 for Mac OS.

SOMAscan® Proteomic discovery platform analysis

SOMAscan®, an aptamer-based proteomics assay, was used to measure 1305 human protein analytes in plasma (SomaLogic, Inc; Boulder, CO, USA). The platform technology is described in Candia et al.[22]. Sample data was normalized to remove hybridization variation within a run. Overall scaling was performed on a per-plate basis to remove overall intensity differences between runs. This was followed by median normalization across the different sample types to remove other assay biases within the run. The statistical analysis of SOMAscan® results was performed using R Studio (R Core Team, 2020), also using a specifically developed webtool for basic data plotting and analysis[66]. For each group comparison, top up- and downregulated proteins have been identified by selecting all the proteins with FDR<0.05 and p value<0.05, and then ordering them according to increased or decreased fold change, expressed in a log2 scale. Pathway enrichment analysis was performed on differentially expressed biomarkers between the groups (pCOVID-19, MIS-C, pHC), using the Molecular Signatures Database v7.4, part of the Gene Set Enrichment Analysis (GSEA) software, a joint project of UC San Diego and Broad Institute.

Biomarker interaction analysis

The potential interactions between all variables in the biomarker and timeline data (MIS-C samples only) were characterized by first scaling the values of each variable (with the scale function in R); then, Pearson correlation coefficients and random forest regression based interaction strengths between the variables were computed. The latter approach allowed us to integrate the biomarker levels with the timeline variables in a multivariate setting, while taking into account the potential linear and nonlinear interactions between all variables.

Pearson correlation coefficient values were computed using the corr.test function (psych package in R). Biomarkers and the time interval variables were ordered by hierarchical clustering (with complete linkage) based on their overall correlation patterns that were visualized with the corrplot function (corrplot package in R).

Random forest regression models were built to compute the interactions between biomarker levels, gene usage, and timeline variables with GENIE3 (Gene Network Inference with Ensemble of trees)[67] using scaled inputs. Each model was composed of 1000 decision trees that collectively predict a given variable's value using all remaining variables as predictors. GENIE3 algorithm also identifies a predictive importance value of a given predictor in each predictor-target pair, which is also referred to as the interaction strength[67]. The median predictive importance value (derived by GENIE3) was extracted from the importance distribution associated with each predictor *versus* all its targets in either treatment condition (glucocorticoids alone, or glucocorticoids + IVIG). The resulting values were visualized using the pheatmap and Complexheatmap packages in R. The variables were clustered based on the median interaction strength (or predictive importance) per variable, by implementing agglomerative hierarchical clustering with Euclidean distance and average linkage.

Author Manuscript Author Manuscript Author Manuscript Author Manuscript

HLA typing

Genomic DNAs were extracted from patients' whole blood using the QIAsymphony DNA Midi Kit and quantified using a fluorescence dye-based assay (PicoGreen dsDNA reagent) by a microplate reader (Molecular Devices SpectraMax Gemini XS). Whole genome sequencing libraries are generated from fragmented DNA using the Illumina TruSeq DNA PCR-Free HT Library Preparation Kit with minor modifications for automation (Hamilton STAR Liquid Handling System) and IDT for Illumina TruSeq DNA UD Indexes (96 Indexes, 96 Samples) adapters. Sequencing libraries were quantified using the KAPA qPCR Quantification Kit (Roche Light Cycler 480 Instrument II) and combined as 24-plex pools after normalization and sequencing on an Illumina NovaSeq 6000 using a S4 Reagent Kit (300 cycles) using 151+8+8+151 cycle run parameters. Primary sequencing data was demuxed using the Illumina HAS2.2 pipeline and sample-level quality control for base quality, coverage, duplicates, and contamination (FREEMIX < 0.05 by VerifyBamID) was conducted. All sequencing data were then processed with Burrows–Wheeler Aligner (BWA) and the Genome Analysis Toolkit (GATK) best-practice pipeline for alignment and variant call. Samples underwent whole genome sequencing at >=30X median depth. Raw fastq files were trimmed using Trimmomatic v0.39[68] and mapped to the hg38 human reference genome using BWA-MEM v07.17. PCR Duplicates were marked using Samblaster v0.1.2.5[69] and GATK4 v4.1.9.0 was used to perform BAM recalibration, and HLA*LA[70] was used to call HLA genotypes. Ethnicity was computed from whole genome sequencing data by Peddy using 2504 thousand genome samples as background.

Bulk TCR and BCR Repertoire

The CDR3 regions of *TRB* and *IGH* rearrangements present in PBMC samples were sequenced in a high-throughput manner using the ImmunoSEQ assay after amplification of the extracted DNA in a bias-controlled multiplex PCR. The resulting CDR3 sequences were collapsed and filtered to quantify the absolute abundance and frequency of each unique CDR3 region with Adaptive Biotechnologies' pipeline[71].

SHM rate was computed by first matching the germline sequences to IMGT gene identification, flagging the IGH assay mutations (mismatches) to V-gene segments as SHM in the same pipeline. Then, the number of detected SHMs was divided with the number of nucleotides in the region where each SHM set is observed (V gene region) to compute the fraction of clonotypes with >1% SHM rate per nucleotide.

We computed the bulk TCR and BCR repertoire statistics, including gene usage, using Immunarch[72]. Gene usage was defined as the fraction of unique clonotypes per sample in which a given gene is present. SARS-CoV-2-specific breadth and depth of each sample was computed using the approach described in Snyder et al.[71] by utilizing the SARS-CoV-2-specific CDR3 sequences previously reported in the ImmuneCODE database[73].

The R package ggpubr was used for visualization of the results with violin, bubble, box, and density plots, whereas the non-parametric Wilcoxon rank sum and Kruskal-Wallis testing and Pearson correlation calculations (along with regression lines showing the

Author Manuscript Author Manuscript Author Manuscript Author Manuscript

95% confidence intervals) were also performed with ggpubr. The reported p-values and significance levels are based on two-tailed testing.

CITE-seq experimental methods

a) Single cell CITE-seq processing—Frozen PBMC samples were thawed, recovered and washed using RPMI media with 10% FBS and 10mg/mL Dnase I (STEMCELL) and then processed as previously described[25] for CITE-seq staining. In brief, samples from different donors were pooled and different timepoints from the same donor were pooled separately so that each pool contains only one timepoint from one donor. PBMC pools were Fc blocked (Human TruStain FcX, 1:10 dilution, BioLegend) and stained with Biotinylated SARS-CoV-2 S1 protein (0.4μg, Acro Biosystems), Totalseq-C human 'hashtag' antibodies (1:100 dilution, BioLegend), and TotalSeq-C PE Streptavidin (1:500 dilution, Biolegend), then washed with staining buffer (2% BSA in PBS). A fraction of the combined cells was used for sorting non-naïve T and B cells (see below). For the unsorted cell fraction, hashtagged PBMC pools were combined and cells were stained with a cocktail of TotalSeq-C human lyophilized panel (BioLegend) of 188 surface proteins (plus 4 isotype controls, See: repository file #10, 50μL reconstitution for 1 million cells staining). Then, cells were washed, resuspended in PBS, and counted before proceeding immediately to the single cell partition step.

b) Sorting of non-naïve B- and T-cell populations—Pooled PBMC samples from different donors were washed with PBS and incubated with Zombie Red Fixable viability dye (1:1000 in PBS, BioLegend, San Diego, CA) for 20 minutes at 4°C protected from light. Then cells were washed with flow staining buffer (10% FBS in PBS) and Fc blocked (Human TruStain FcX, BioLegend) for 15 minutes on ice. The fluorescence-labeled antibody cocktail against human CD45 (APC/Cyanine7, CD3 (AF488), CD19 (APC), CCR7 (BV786), CD95 (BV650), IgD (PerCP-Cy5.5) and CD27(PE/Cyanine7; all antibodies obtained from Biolegend, and all used at 1:20 dilution) were added at the end of blocking and incubated for 20 minutes at 4°C in the dark. Cells were washed and sorted on a BD Aria sorter (BD Biosciences, San Jose, CA) in Biosafety Level 3 (BSL3) lab. Non-naïve B cell population were gated by $CD45^+CD19^+IgD^-$ or $CD27^+$ and non-naïve T cell population were gated by $CD45^+CD3^+CCR7^{low}$ or $CD95^+$.

c) Single cell RNA sequencing—PBMC samples were partitioned into single cell Gel-Bead in Emulsion (GEM) mixed together with the reverse transcription (RT) mix using 10× 5' Chromium Single Cell Immune Profiling Next GEM v1.1 chemistry (10x Genomics, Pleasanton, CA), as previously described[25]. The RT step was conducted in the Veriti Thermo Cycler (ThermoFisher Scientific, Waltham, MA). Single cell gene expression, cell surface protein, T cell receptor (TCR) and B cell receptor (BCR) libraries were prepared as instructed by 10x Genomics user guides (https://www.10xgenomics.com/resources/user-guides/). All libraries were quality controlled using Bioanalyzer (Agilent, Santa Clara, CA) and quantified using Qubit Fluorometric (ThermoFisher). 10x Genomics 5' Single cell gene expression, cell surface protein tag, TCR and BCR libraries were pooled and sequenced on Illumina NovaSeq platform (Illumina, San Diego, CA) using the sequencing parameters recommended by the 10x Genomics 5' v1.1 user guide.

Author Manuscript Author Manuscript Author Manuscript Author Manuscript

d) Bulk RNA sequencing and single cell sample demultiplexing—For each sample, 100,000–500,000 cells were processed in Trizol using the miRNAeasy micro kit (Qiagen, Germantown, MD) and standard RNA sequencing libraries were generated using Illumina Truseq library preparation kits. The results of bulk RNA sequencing were used for demultiplex of CITE-seq samples by generating SNP calls for each donor. Sequencing results were demultiplexed and converted to FASTQ format using Illumina bcl2fastq software. The sequencing reads were adapter and quality trimmed and then aligned to the human genome using the splice-aware STAR aligner and SNP calls were generated using the previously published protocol[74]. The software package *demuxlet* was used to then match single cell gene expression data to each donor and identify empty droplets and doublets. Because multiple samples from different timepoints for each donor were collected and could not be demultiplexed by this method alone, 'hashtag' antibodies (Biolegend) were used to uniquely label the different time points.

CITE-seq quantification and statistical analysis

a) Single cell data processing and clustering—The single cell data processing, CITE-seq protein data denoise and clustering were performed as described before[25]. Specifically, CellRanger (10x Genomics) version 3.1.0 was used to map cDNA libraries to the hg19 genome reference and to count antibody tag features. Data were further processed using *Seurat* (v.3.1.0) running in R v3.6.1. After filtering to single cell based on *demuxlet* output, we further demultiplexed the timepoints using the hashtag antibody staining. We removed cells with less than 250 or greater than 4,000 detected genes, greater than 20% mitochondrial reads, cell surface protein tag greater than 200,000, and hashtag antibody counts greater than 50,000. The protein data was normalized and denoised using the DSB method[75]. The following parameters were used in the dsb normalization function: define.pseudocount = TRUE, pseudocount.use = 10, denoise_counts = TRUE, use.isotype.control = TRUE. The DSB-normalized protein data, excluding the isotype control antibodies, were used to generate the Euclidean distance matrix computed for all single cells. Then the shared nearest neighbor graph followed by k-nearest neighbors clustering were built using the *FindNeighbors* and *FindClusters* functions in Seurat (v3.1.0), respectively. Major cell clusters were then manually annotated using the surface protein together with gene expression. Major cell clusters identified based on protein expression profile and shown in Figure 4a included: B_Mem: Memory B cells; CD4_Mem: Memory CD4 T cells; CD8_Mem: Memory CD8 T cells; CD4_isobinding: isotype antibodies binding CD4 T cells; cDC: Conventional dendritic cells; cKit+CD3- activated: cKit high cells with enrichment of activated T cell signatures, but lack surface CD3, CD4 and CD8 expression; dim: low quality, cell subsets with high mitochondria/ribosome genes and most surface markers lowly expressed; DNT: Double negative T cells; HSC: Hematopoietic stem or progenitor cells; MAIT: Mucosal-associated invariant T cells; Mono_Classical/Intermediate/NonClassical: Classical/Intermediate/NonClassical Monocytes; NK_CD16hi/NK_CD56hiCD16lo: CD16 highly expressed/CD56 highly and CD16 lowly expressed natural killer cells. pDC: Plasmacytoid DC; RBC: Red blood cells.

b) Label transfer for cell annotations—To compare the cell population frequencies directly with aCOVID-19 patients and avoid potential annotation batch effect, the previously

Author Manuscript Author Manuscript Author Manuscript Author Manuscript

published aCOVID-19 dataset[25] was projected onto CITE-seq data—query from this experiment in Seurat (v3.1.0) using *FindTransferAnchors* function. Log normalization and first 30 PCs were used for the integration. Cell annotations were then predicted using *TransferData* function and the predicated labels were added to the metadata as *predicated.id* column.

c) Pseudobulk differential expression and gene set enrichment analysis— Pseudobulk gene differential expression analysis and gene set enrichment analysis were performed as described before[25]. Briefly, all unsorted cells in a given sample were computationally "pooled" according to their cluster assignment by summing all reads for a given gene. Pseudobulk libraries made up by few cells and therefore likely not modeled properly by bulk differential expression methods were removed from analysis for each cell-type separately to remove samples that contained fewer than 5 cells and less than 40,000 unique molecular identifier counts detected after pooling. Lowly expressed genes were removed for each cell type individually using the filterByExpr function from *edgeR*[76]. Differentially expressed genes were identified using the *limma voom*[77] workflow which models the log of the cpm (counts per million) of each gene. Scaling factors for library size normalization were calculated with the calcNormFactors function with method = "RLE". Genes were ranked using the moderated T statistics for the relevant coefficient from the *limma voom* model. Enriched gene sets were identified using the pre-ranked GSEA algorithm implemented in the *fgsea* R package. Gene set list used for enrichment assessment (including GO BP, KEGG, Reactome, MSigDB'sHallmark collection, Blood Transcriptomic Modules and a few published datasets) were the same as described in Liu et al.[25]. P values were adjusted using the Benjamini-Hochberg method for the whole gene set list. Selected pathways shown in figures were manually curated to select gene sets relevant to immunology and often enriched in several cell-types across the various differential expression comparisons.

d) Models used for differential expression: MIS-C and pCOVID-19 patients versus pHCs—Using the pseudobulk *limma voom* workflow as described in "*Pseudobulk differential expression and gene set enrichment analysis*", differentially expressed genes between patient samples (with admission days < 41) and pHC were identified with a model with the following formula in R: ~ 0 + mis-c_vs_pediatric_healthy + age and ~ 0 + pediatric_covid_vs_healthy + age, where patient_vs_healthy is a factor variable with two levels. The contrasts.fit function was then used to compare the estimated means between patients and pediatric healthy controls.

e) Models used for differential expression: MIS-C patients vs. pediatric COVID-19 patients—Similarly, differentially expressed genes between MIS-C samples (with admission days < 41) and pediatric COVID-19 were identified with a model with the following formula in R: ~ 0 + mis-c_vs_pediatric_covid + days_since_admission + age, where mis-c_vs_pediatric_covid is a factor variable with two levels, time effect was considered using the days_since_admission term. The contrasts.fit function was then used to compare the estimated means between MIS-C and pediatric COVID-19.

Author Manuscript Author Manuscript Author Manuscript Author Manuscript

f) Models used for differential expression: time effect of MIS-C patients and COVID-19 patients gene expression—Differentially expressed genes of MIS-C samples and pediatric COVID-19 samples associated with time respectively, were identified with a model with the following formula in R: ~ days_since_admission + age. The contrasts.fit function was then used to estimated changes associated with disease time course of MIS-C and pediatric COVID-19 respectively.

g) Gene set module scores Calculation—Selected module scores (gene set signature score) representing enriched pathway activities were calculated for each sample as reported before[25]. Specifically, leading edge genes identified by GSEA from the MIS-C *versus* pCOVID-19 model above were used to enhance signal-to-noise ratio and highlight mainly the differences between MIS-C *versus* pCOVID-19. The pseudobulk gene counts were normalized with the *varianceStabilizingTransformation* function from Deseq2[78] for the score calculation. The scores were generated using gene set variation analysis (GSVA) method from the GSVA R package.

h) TCR and BCR data processing—*CellRanger* (10x Genomics) version 3.1.0 was used to assemble V(D)J contigs (https://support.10xgenomics.com/single-cell-vdj/software/pipelines/latest/algorithms/annotation). For TCR data, the V(D)J assignment and clonotype were from 10x *CellRanger* output of the filtered_contig_annotations.csv file. For BCR data, V(D)J sequencing contigs from 10x *CellRanger* output was processed using Immcantation v3.0.0 toolbox (https://immcantation.readthedocs.io/en/latest/index.html). IgBLAST and IMGT germline sequence databases and Change-O package[79] were used for sequence alignment and V(D)J annotations. BCR sequence genotype inference and mutation load quantification were performed with reference to the pipeline from Mathew et al.[80] using the TIgGER R package[81] and ShazaM R package[79]. The TCR and BCR sequence data, contig assignments and estimated BCR mutation frequencies were combined respectively using *scRepertoire* R package and integrated with the single-cell RNA-seq Seurat object in the metadata.

i) CITE-seq data visualization—For heatmaps showing pseudo-bulk gene expression profiles, the log of counts-per-million for each sample and gene for a given cell-type was calculated by pooling cells as described in "*c) Pseudobulk differential expression and gene set enrichment analysis*". Library size normalization was performed without additional scaling factors and heatmaps were scaled to z-score among samples for each gene. *ComplexHeatmap*[82] and *pheatmap* were used for plotting heatmaps using R. The *ggplot2* and *ggpubr* R packages are used for box, bubble and scatter plots visualization.

j) Validation of gene set enrichments in external scRNA-seq data from Ref.13—Single cell data from the cohort of Ramaswamy et al. *Immunity*, 2021[13] was downloaded from fastgenomics (the Ramaswamy2021_MIS-C_10x_PBMC dataset). Using the pre-annotated cell clusters from the original publication, single cell gene expression data were pooled into pseudobulk libraries and differential expression and gene set enrichment analyses of MIS-C patients *versus* pHCs were done as described in "*c) Pseudobulk differential expression and gene set enrichment analysis*" and "*d) Models used*

Author Manuscript Author Manuscript Author Manuscript Author Manuscript

for differential expression: MIS-C patients and pediatric COVID-19 patients versus pHCs"; age was included in the model as a covariate.

HuProt™ Autoantibody analysis

Autoantibody analysis was performed using HuProt™ v4.0 human protein microarrays and processed by CDI Laboratories (Baltimore, MD). IgG profiling was performed for 15 serum samples from 5 children with pCOVID-19 and 10 children with MIS-C, of whom 4 had received IVIG. Briefly, the arrays were blocked and probed with the samples at a 1:1,000 dilution and incubated at room temperature for 1 hour. Then the arrays were washed and probed with Alexa-647-anti-human-IgG (Fc) for signal detection as previously described. Utilizing CDI software, quantile normalization of the raw signal intensities (F635 median for IgG; F532 median for IgA) was performed on all arrays. The data of several proteins that directly bind with secondary antibodies detected through buffer incubation without any serum were excluded (such as IGHG1, IGHG3 and so on) alongside the controls (such as Rhodamine+IgG64, Anti-human IgG, GST 10ng/ul etc.). The quantile normalized IgG binding intensities of the remaining 23,040 protein targets were then visualized using the Morpheus, https://software.broadinstitute.org/morpheus. The t-test was used to compare the different groups and candidates were identified using the following criteria: the variance for the data points was greater than 10,000,000, the fold-change of average signal intensity was greater than 4 between the 2 groups, and the false discovery rate was <0.5.

Multiplex particle-based anti-cytokine autoantibody screening assay and functional evaluation—Plasma samples were screened for autoantibodies against IFN-α, IFN-β, IFN-ω and IFN-γ in a multiplex particle-based assay[83], in which differentially fluorescent magnetic beads were covalently coupled to recombinant human proteins (2.5 μg/reaction). Beads were combined and incubated for 30 minutes with diluted plasma samples (1 to 100 dilution). Beads were then washed and incubated with PE-labeled goat anti-human IgG (1 ug/mL) for an additional 30 minutes. Beads were washed again, resuspended in assay buffer, and analyzed on a BioPlex X200 instrument. Plasma samples with a fluorescence intensity > 1,500 were tested for blocking activity. The blocking activity of autoantibodies was determined by assessing STAT1 phosphorylation in healthy control cells following stimulation with the appropriate cytokines in the presence of 10% healthy control or patient plasma. Surface-stained healthy control PBMCs were cultured in serum-free RPMI medium with 10% healthy control or patient plasma and were either left unstimulated or stimulated with 10 ng/mL of IFN-α, IFN-β, or IFN-ω or 400 units/mL of IFN-γ for 15 minutes at 37°C. Cells were fixed, permeabilized, and stained for intranuclear pSTAT1 (Y701). Cells were acquired on a BD LSRFortessa cytometer, gated on CD14+ monocytes, and analyzed with FlowJo software.

Data Availability Statement

Source data and Supplementary Datasets are provided for Figures 1–5; Extended Data Fig. 1–7. CITE-Seq and single-cell TCR and BCR repertoire data have been deposited on Zenodo, with the following link: https://zenodo.org/record/5524378#.YUzcFy1h3GJ.

Author Manuscript Author Manuscript Author Manuscript Author Manuscript

Bulk TCR/BCR repertoire data are available at the following link: https://clients.adaptivebiotech.com/pub/sacco-2021-misc using the following login credentials: email: sacco-review@adaptivebiotech.com; password: sacco2021review.Whole genome sequencing data that were used for inputting HLA typing are accessible at phs002245.v1: Genetic Determinants of Susceptibility to Severe COVID-19 Infection: https://www.ncbi.nlm.nih.gov/projects/gap/cgi-bin/study.cgi?study_id=phs002245.v1.p1

Code Availability Statement

R scripts that were used in the immune repertoire and gene expression analysis are publicly available on Github: https://github.com/cihangenome/multiomics-misc

Author Manuscript
Author Manuscript
Author Manuscript
Author Manuscript

Extended Data

Extended Data Fig. 1: Differences in soluble biomarker levels among pediatric (pCOVID-19), adult COVID-19 (aCOVID-19), and pediatric and adult healthy controls (pHC, aHC).

a, Children with mild pCOVID-19 (n=39) in the first 7 days since symptom onset have significantly higher IFN-α2a levels compared to healthy pediatric controls [pHC] (n=16), healthy adult controls [aHC] (n=40), children with MIS-C (both in the first 7 days since hospitalization: MIS-C Early, n=36) and later in the course of the disease (MIS-C Late, n=32)), and adults with moderate acute COVID-19 (aCOVID-19, n=26). Maxima of box

Author Manuscript Author Manuscript Author Manuscript Author Manuscript

plots represent median values, and bars represent interquartile range. Statistical analysis was performed with Kruskal-Wallis test with adjustment for multiple comparisons.

b-d, Comparison of soluble biomarkers measured within 7 days of symptom onset in children (n=9) and within 7 days of admission in adults (n=26) with moderate acute COVID-19, as well as pHC (n=53) and aHC (n=45), both unadjusted (left graphs, Kruskal-Wallis test) and adjusted for the baseline differences in healthy subjects of the same age group (right graphs, two-tailed Mann-Whitney test). Bars represent median values and interquartile range.

b, Biomarkers whose serum levels were significantly different in pHC and aHC, but not in diseased subjects, indicating that the difference of unadjusted blood levels observed between pCOVID-19 and aCOVID-19 is probably driven by age, rather than COVID-19 itself.

c, Biomarkers that differed significantly in pCOVID-19 vs. aCOVID-19, but not between pHC and aHC, suggesting that the nature and severity of inflammatory responses induced by SARS-CoV-2 infection differentially affects patients of different age.

d, Biomarkers for which both age and SARS-CoV-2 infection independently contributed to differences in levels in children and adults. In all panels, significance is indicated as follows: *, P<0.05; **, P<0.01; ***, P<0.001; ****, P<0.0001.

Author Manuscript Author Manuscript Author Manuscript Author Manuscript

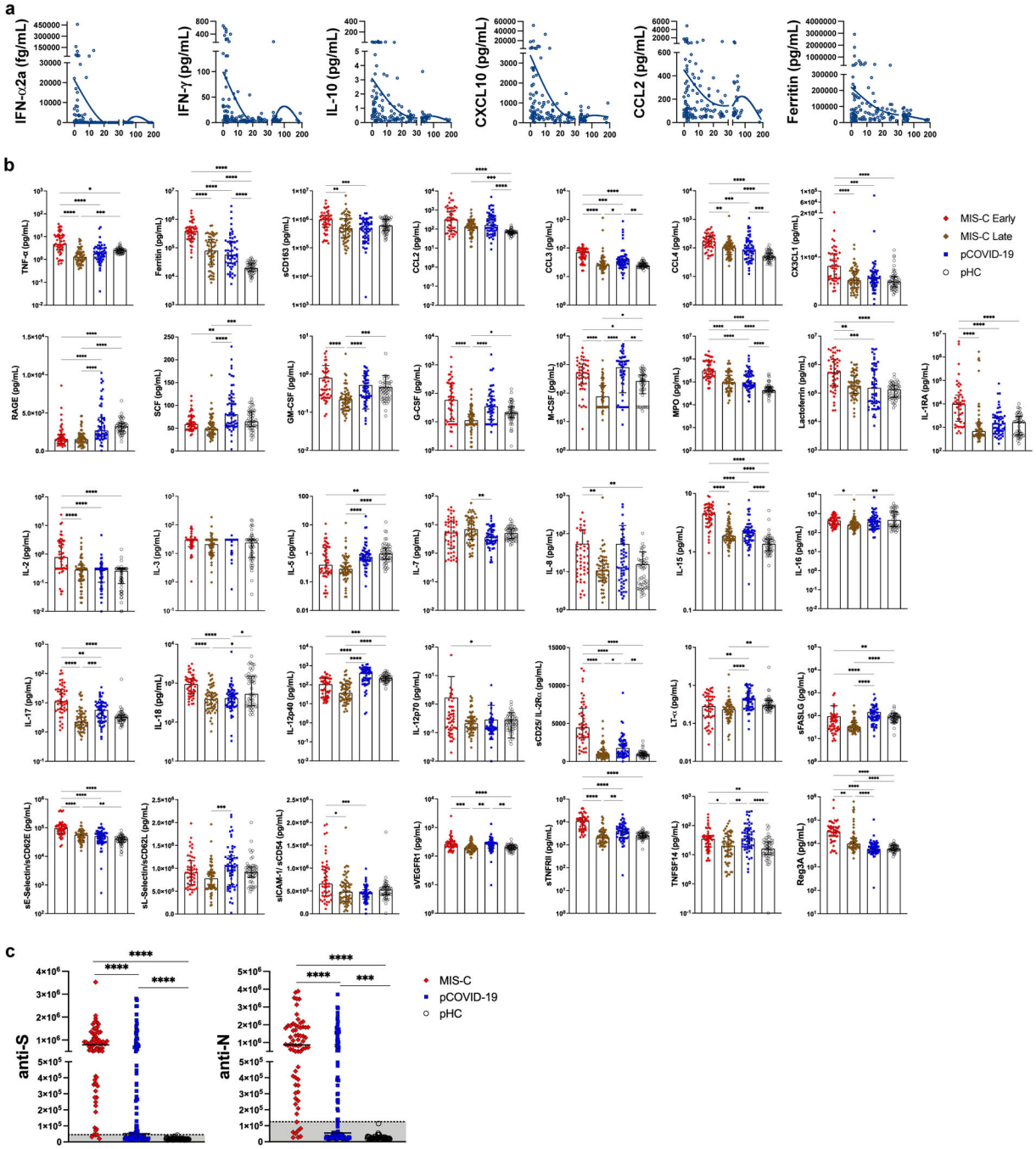

Extended Data Fig. 2: Profile of soluble biomarkers and results of COVID-19 serology in pediatric COVID-19 (pCOVID-19), children with MIS-C and pediatric healthy controls (pHC).

a, Analysis of IFN-α2a, IFN-γ, IL-10, CXCL10, CCL2 and ferritin levels over time in 110 pCOVID-19 patients, for 34 of which more than one sample was obtained during hospitalization. The X-axis shows time from onset of symptoms or (for asymptomatic children) positive PCR.

b, Comparison of serum biomarker levels in children with early (n=48, within 7 days since admission) and late (n=60, >7days) MIS-C, pCOVID-19 within 7 days from symptom

Author Manuscript Author Manuscript Author Manuscript Author Manuscript

onset (n=57) and pHC (n=53). Median values with IQR are shown. Univariate analysis by Kruskal-Wallis test with adjustment for multiple comparisons. P values are marked as follows: * <0.05, ** <0.01, *** <0.001, **** <0.0001.

c, Levels of anti-Spike (anti-S) and anti-Nucleocapsid (anti-N) antibodies in MIS-C (n=68) and pCOVID-19 (n=104) patients and in pHC (n=53). Blood samples were obtained at a median of 4 days after hospitalization (IQR, 1.75–13 days) for MIS-C patients, and at a median of 3 days (IQR, 1–14 days) after onset of symptoms or positive PCR for pCOVID-19 patients. Values are expressed in Light Units. Positive values are shown above the grey areas. Positivity cut-off values are 45,000 for anti-S, and 125,000 for anti-N antibodies, respectively. Statistical analysis was done with Mann-Whitney test with two-tailed P values. ***, P<0.001; ****, P<0.0001.

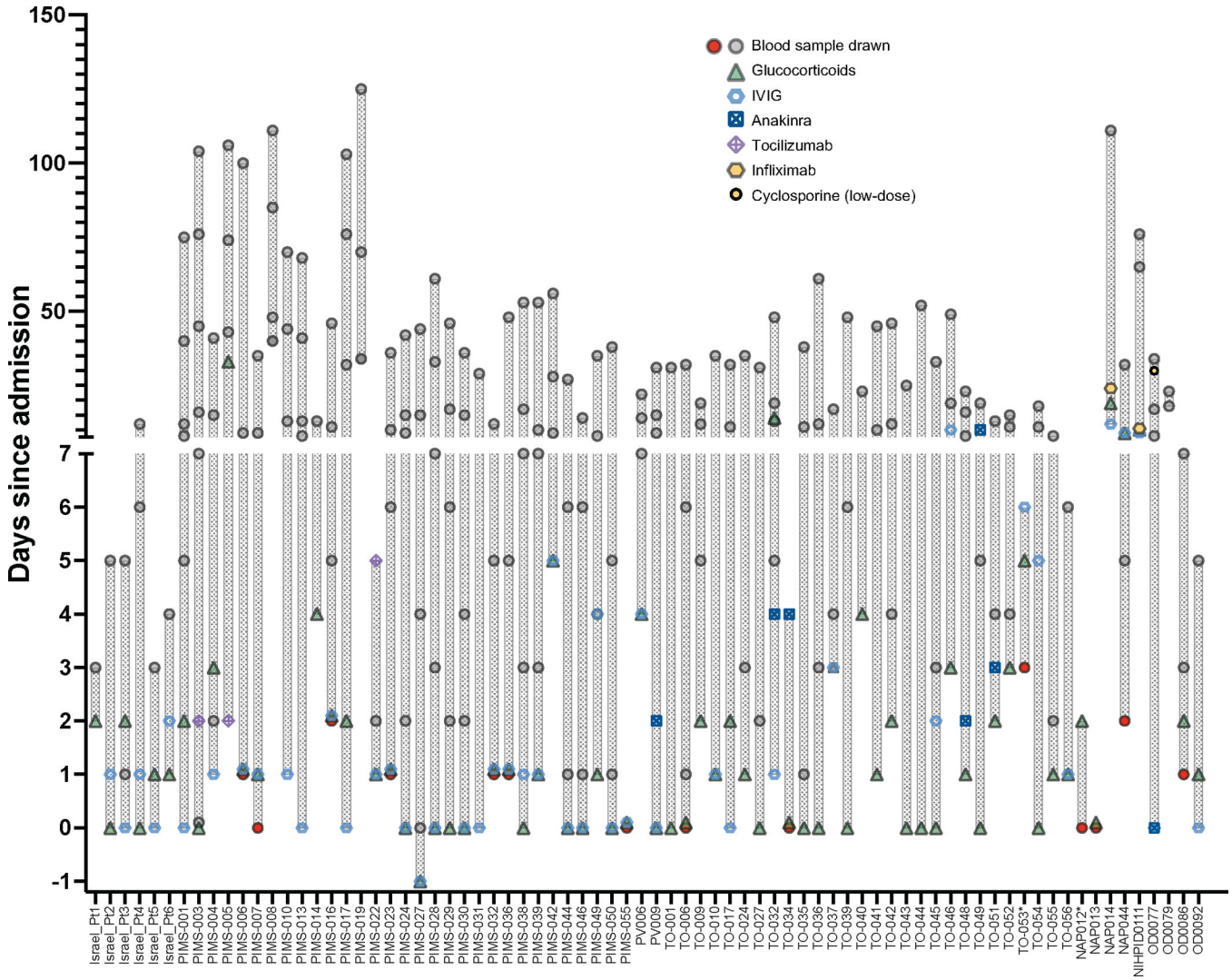

Extended Data Fig. 3: Schematic diagram of timing of blood sample collection and administration of therapeutic modalities compared to day of admission (day 0) in MIS-C patients.

Author Manuscript Author Manuscript Author Manuscript Author Manuscript

Red circles identify first blood samples collected prior to administration of glucocorticoids, IVIG or biologics. For PIMS-006, PIMS-016, PIMS-023, PIMS-032, PIMS-036, PIMS-055, TO-006, TO-034, NAP013, the first blood sample was obtained the same day (and immediately prior to) therapeutic interventions with glucocorticoids, IVIG and/or biologics were started. *Levels of soluble biomarkers were not measured in the first blood samples obtained from NAP012 and TO-053.

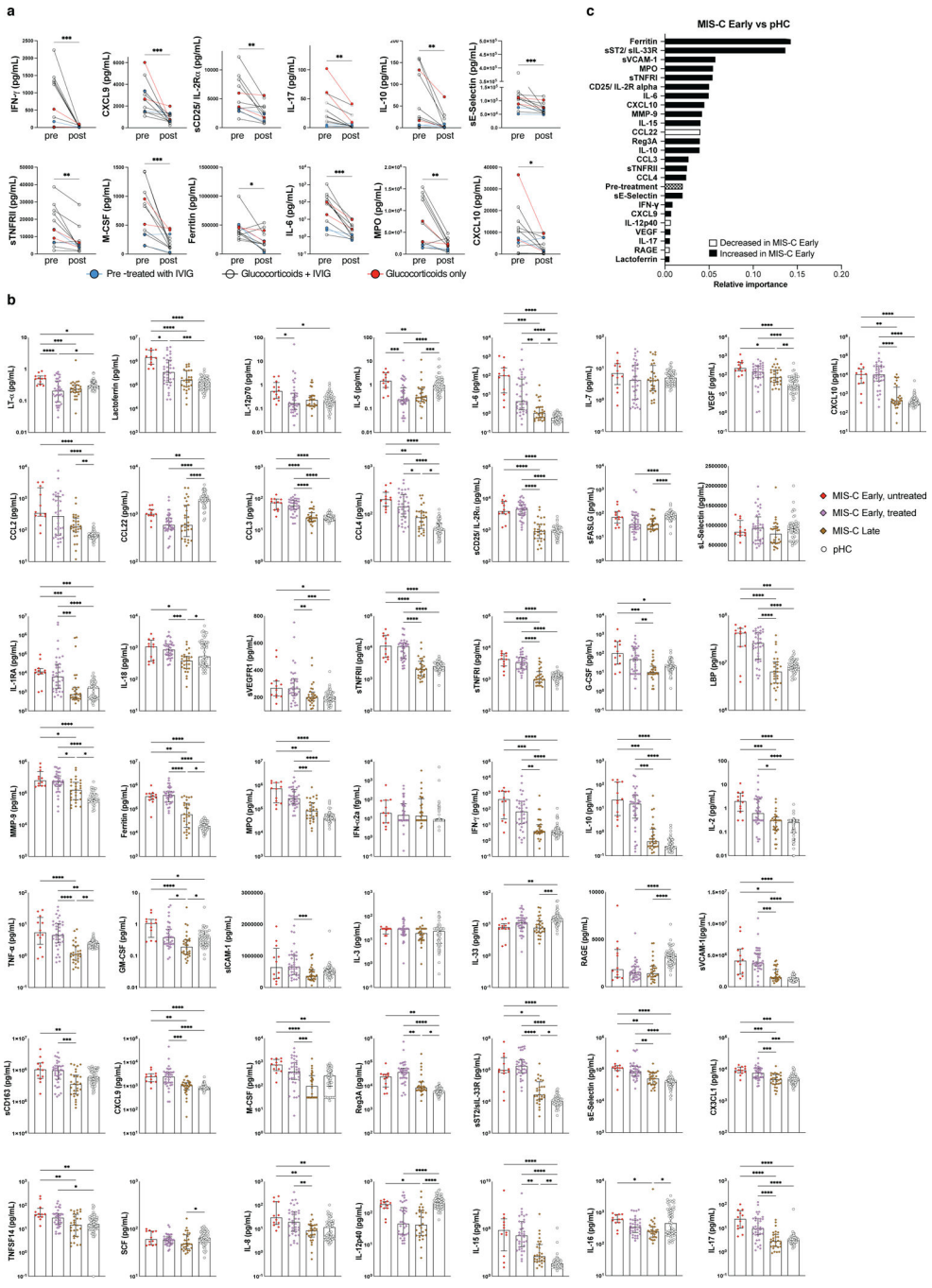

Extended Data Fig. 4: Effect of treatment on levels of soluble biomarkers in MIS-C.

Author Manuscript Author Manuscript Author Manuscript Author Manuscript

a, Biomarker changes following systemic glucocorticoids in 12 MIS-C patients. Samples were drawn at a median of 0 days (IQR −1 to 0) prior to (left) and 5 days (IQR 4 to 7.5) after (right) treatment with glucocorticoids and IVIG (black lines) or glucocorticoids alone (red lines). Two patients (indicated by blue circles and lines) had received IVIG prior to blood sampling. Wilcoxon matched-pairs signed rank test with two-tailed P value was used for comparisons. *p<0.05, **p<0.01, ***p<0.001.

b, Comparison of soluble biomarker levels in MIS-C Early children (within 7 days since admission) who had not (untreated, n=12) and in those who had (treated, n=36) received glucocorticoids and/or IVIG prior to blood sampling. Results are compared to levels in MIS-C Late (>7 days since admission) patients (n=60) and pediatric healthy controls (pHC, n=53). Maxima of box plots represent median values, and bars represent interquartile range. Statistical analysis was performed by Kruskal-Wallis test with adjustment for multiple comparisons. P values are marked as follows: * <0.05, ** <0.01, *** <0.001, **** <0.0001.

c, Random forest classification comparing MIS-C Early (n=46) to pHC (n=52), with treatment prior to blood sampling included among the variables. The sample cohort is the same as in Figure 2e.

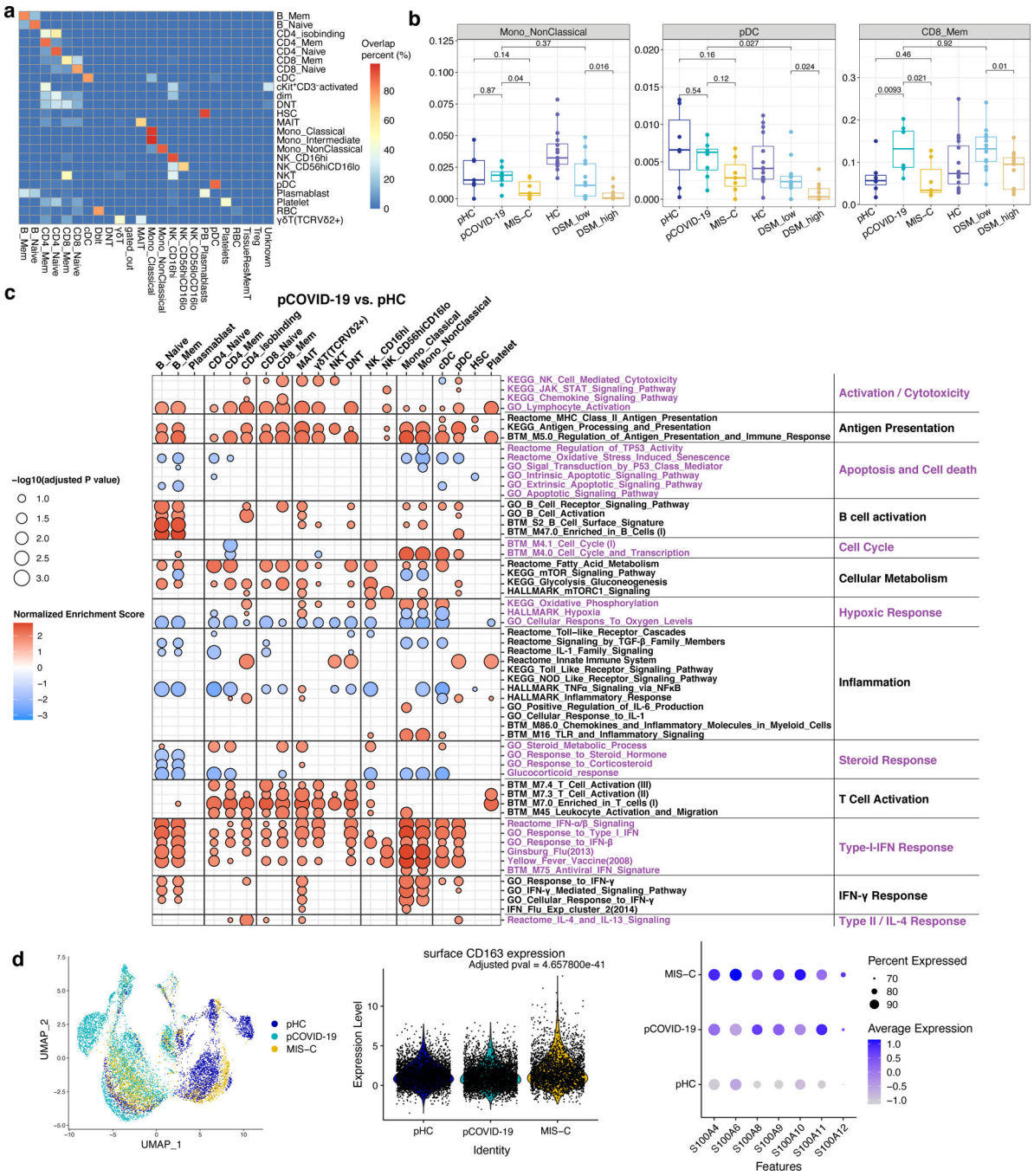

Extended Data Fig. 5: Immune cell atlas and cell-type specific gene expression profile of MIS-C and pediatric COVID-19 (pCOVID-19).

a, CITE-seq label transfer from previous adult COVID-19 experiments. Heatmap shows the overlap percentage of predicted markers from label transfer (x-axis) and annotated cell populations in this pediatric dataset (y-axis).

b, Frequencies of immune cell clusters for non-classical monocytes, plasmacytoid dendritic cells (pDC) and CD8 memory T cells in adult healthy controls (aHC, n=13), adult patients with less severe (disease severity matrix low, DSM_low, n=13) COVID-19, adult patients

Author Manuscript Author Manuscript Author Manuscript Author Manuscript

Author Manuscript Author Manuscript Author Manuscript Author Manuscript

with more severe (DSM_high, n=13) COVID-19, pediatric HC (pHC, n=7), pediatric COVID-19 (pCOVID-19,n=8) and MIS-C patients (n=7). P values shown were obtained using two-sided Wilcoxon test between indicated two groups. Adult COVID-19 data are from Liu et al, 2021 (ref.25). To avoid potential batch effects of independently annotated adult and pediatric populations, cell frequencies of pediatric dataset shown were obtained by label transfer from adult data (See Methods and panel a). Each dot indicates a subject. Only the first timepoint from each subject is shown. Box plot elements are the same as in Figure 4e.

c, Enrichment Analysis of pCOVID-19 (n=7) vs. pHC (n=7) at timepoints within 40 days of admission. Selected gene sets are grouped into functional/pathway categories. Dot color denotes normalized gene set enrichment score and size indicates –log10(adjusted p value). P values were adjusted using the Benjamini-Hochberg method.

d, From left to right: UMAP of monocyte RNA expression clusters, surface CD163 expression (FDR adjusted p value comparing surface CD163 expression of MIS-C monocytes vs. pHC and pCOVID-19 monocytes is shown) and expression of S100A family inflammatory genes which are differentially expressed in monocytes of MIS-C versus pHC. Cells from all time points are shown (pHC, n=7; pCOVID-19, n=8; MIS-C, n=10, with two timepoints included for 3 MIS-C patients).

Author Manuscript Author Manuscript Author Manuscript Author Manuscript

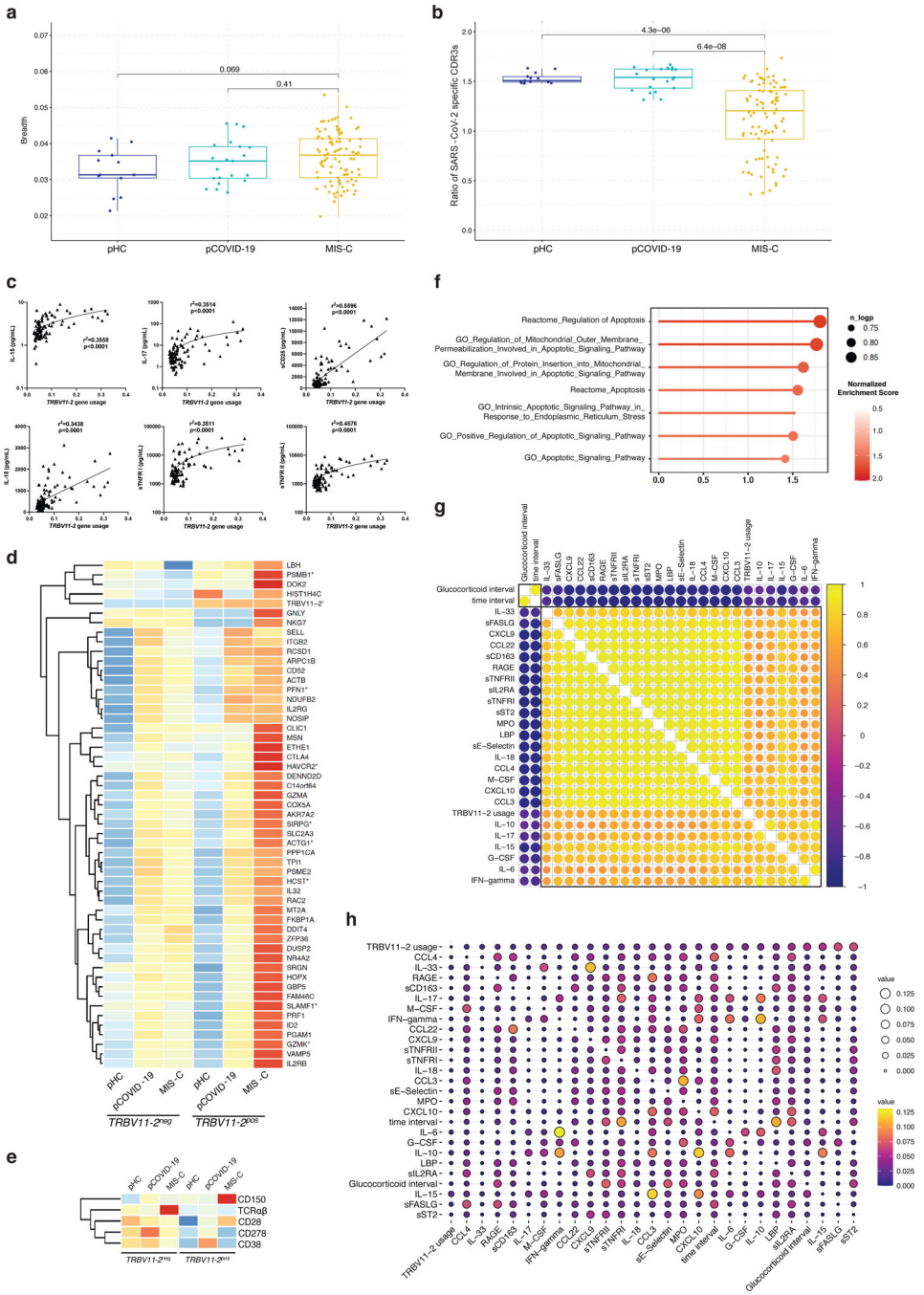

Extended Data Fig. 6: SARS-CoV-2 specific clonotypes, characteristics of *TRBV11–2*+ clonotypes, and correlation with soluble biomarkers.

a, Breadth of SARS-CoV-2 specific TRB clonotypes in pHC, pCOVID-19 and MIS-C patients.

b, Ratio of SARS-CoV-2 specific CDR3 clonotypes among unique *TRBV11–2*-positive versus *TRBV11–2*-negative clonotypes in pHC, pCOVID-19 and MIS-C.

c, Simple linear regression analysis, correlating frequency of *TRBV11–2* clonotypes and soluble biomarker levels. R squared goodness of fit and p values are shown.

Author Manuscript Author Manuscript Author Manuscript Author Manuscript

d, Gene expression of *TRBV11–2* positive (*TRBV11–2*^{pos}) compared to *TRBV11–2* negative (*TRBV11–2*^{neg}) CD4+ T cells within MIS-C samples (n=10, 3/7 patients with 2 time points). Differentially expressed genes with adjusted p value < 0.2 are marked with an asterisk (*). Scaled average gene expression level of *TRBV11–2*^{neg} and *TRBV11–2*^{pos} CD4+ T cells is shown in all 3 groups (pHC, pCOVID-19, and MIS-C).

e, Heatmap showing the marker genes of *TRBV11–2*^{pos} MIS-C CD4+ T cells compared to *TRBV11–2*^{neg} CD4+ T cells.

f, Gene set pathway enrichment analysis (GSEA) of apoptosis signature in *TRBV11–2*^{pos} CD4+ T cells from MIS-C patients (n=7, 3/7 patients with 2 time points). Dot color denotes normalized gene set enrichment score and size indicates –log10(adjusted p value). P values were from GSEA test of the whole gene sets (see: Methods) and adjusted using the Benjamini-Hochberg method.

g, Pearson correlation coefficient values between indicated variables. The top 50th percentile predictors of *TRBV11–2* gene usage are shown. Analysis conducted on 92 samples collected at various timepoints after hospitalization from 56 MIS-C patients who received glucocorticoids. Time interval and glucocorticoid interval are defined as days since admission and since initiation of systemic glucocorticoids, respectively.

h, Pairwise interaction strengths derived from random forest regression analysis. Columns identify predictors, and rows correspond to targets. Input data are the same as in panel f.

In panels **a** and **b**, values are for 21 samples from 21 pCOVID-19, 96 samples from 58 MIS-C, and 13 samples from 13 pHC subjects. Box plots show the median, first and third quantiles (lower and upper hinges) and smallest (lower hinge - 1.5*interquartile range) and largest values (upper hinge + 1.5* interquartile range) (lower and upper whiskers). Statistical analysis was done with two-tailed Wilcoxon test. In panels **d** and **e**, average log fold change (logFC) threshold 0.2 and p value 0.2 were used for marker gene cutoff, and P values were calculated using the Wilcoxon Rank Sum test and adjusted using FDR method.

Author Manuscript Author Manuscript Author Manuscript Author Manuscript

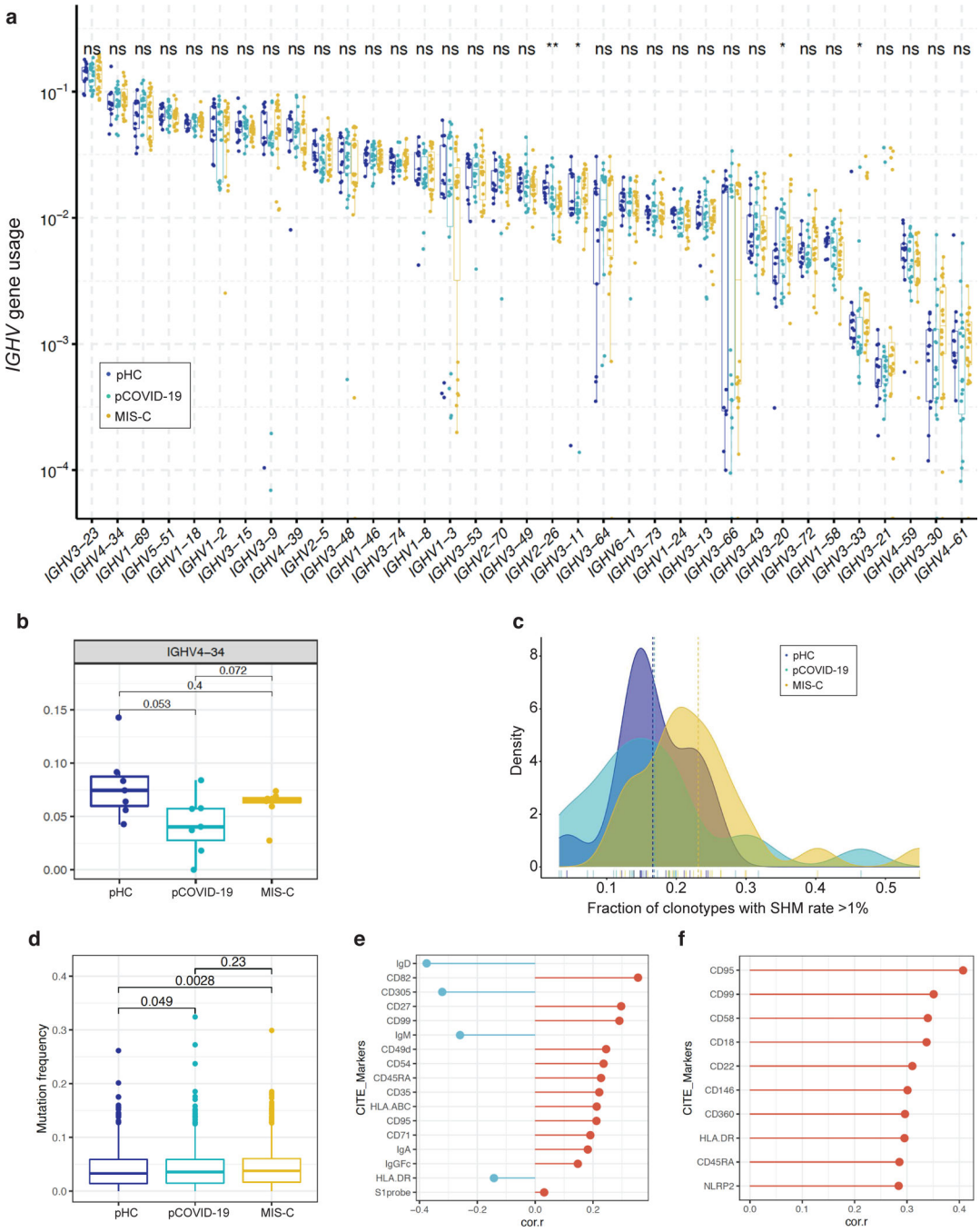

Extended Data Fig. 7: *IGHV* gene usage, mutation frequency and surface markers associated with mutation frequency.

a, Usage of *IGHV* genes in pediatric healthy controls (pHC, n=13 samples from 13 subjects), children with acute COVID-19 (pCOVID-19, n=18 samples from 15 patients) and MIS-C (n=23 samples from 19 patients). ns, not significant; *,p≤0.05; **p≤0.01; ***, p≤0.001; ****, p≤0.0001. Statistical analysis was done with Kruskal-Wallis test with unadjusted P values, with box plot showing the median, first and third quantiles (lower and

Author Manuscript Author Manuscript Author Manuscript Author Manuscript

upper hinges) and smallest (lower hinge - 1.5*interquartile range) and largest values (upper hinge + 1.5* interquartile range) (lower and upper whiskers).

b, Frequency of *IGHV4–34* B cell clonotypes in pHC (n=7), pCOVID-19 (n=8) and MIS-C (n=8, 2 of which with 2 timepoints) within 40 days of admission. P values shown were obtained using two-sided Wilcoxon test between indicated two groups. Each dot indicates a sample. Box plot elements are the same as Figure 4e.

c, Fraction of *IGHV* clonotypes with a somatic hypermutation (SHM) rate >1% among unique clonotypes identified by high-throughput sequencing. Unadjusted P values (Wilcoxon rank sum test) were as follows: pHC *versus* pCOVID-19, P=0.514; pHC *versus* MIS-C, P=0.028; pCOVID-19 *versus* MIS-C, P=0.016.

d, Quantification of somatic hypermutation in memory B cells from pHC (n=7), pCOVID-19 (n=8) and MIS-C (n=7, 3 of which with 2 timepoints) patients. P values shown were obtained by applying two-sided Wilcoxon test between indicated two groups. Each dot indicates a cell. Box plot elements are the same as Figure 4e.

e, B cell surface markers correlating with mutation frequency in memory B cells from MIS-C patients. Pearson correlation values are shown (x-axis). Top 10 and a few selected significant markers are shown. S1 probe: SARS-CoV-2 spike protein probe.

f, Plasmablast cell surface markers correlating with mutation frequency from MIS-C patients. Pearson correlation values are shown (x-axis). Top 10 significant markers are shown.

Extended Data Table 1 -

Statistical analysis of differences in individual biomarker levels in 2-group comparisons.

Biomarker	MIS-C (n=48) vs pHC (n=53)	pCOVID-19 (n=57) vs pHC (n=53)	MIS-C (n=48) vs pCOVID-19 (n=57)	Mild (n=45) vs moderate (n=9) pCOVID-19	Moderate COVID-19 in adults (n=26) vs children (n=9)	Adult (n=45) vs pediatric (n=53) HC	Moderate COVID-19 in adults (n=26) vs children (n=9), adjusted for baseline differences in healthy adults and children
IL-6	**<0.001**	**<0.001**	**<0.001**	0.065	**0.011**	0.833	**0.013**
IL-8	**<0.001**	0.053	0.189	0.134	**0.004**	0.184	**0.004**
IL-12p40	**<0.001**	**0.017**	**<0.001**	0.585	0.271	**<0.001**	0.540
IL-15	**<0.001**	**<0.001**	**<0.001**	0.844	0.079	**<0.001**	**0.016**
IL-16	0.434	0.228	0.499	0.092	0.382	**<0.001**	0.403
IL-17	**<0.001**	**0.002**	**<0.001**	0.634	0.255	**<0.001**	**<0.001**
IL-7	0.940	**0.026**	0.269	0.384	**0.004**	**<0.001**	**<0.001**
LT-α	0.338	**0.010**	**0.006**	0.889	0.160	0.666	**0.049**
VEGF	**<0.001**	**0.003**	**<0.001**	0.880	0.301	**<0.001**	0.978
CXCL10	**<0.001**	**0.004**	**<0.001**	0.618	0.934	**0.007**	0.677
CCL2	**<0.001**	**<0.001**	0.061	0.072	**0.004**	**<0.001**	0.934

Author Manuscript Author Manuscript Author Manuscript Author Manuscript

Biomarker	MIS-C (n=48) vs pHC (n=53)	pCOVID-19 (n=57) vs pHC (n=53)	MIS-C (n=48) vs pCOVID-19 (n=57)	Mild (n=45) vs moderate (n=9) pCOVID-19	Moderate COVID-19 in adults (n=26) vs children (n=9)	Adult (n=45) vs pediatric (n=53) HC	Moderate COVID-19 in adults (n=26) vs children (n=9), adjusted for baseline differences in healthy adults and children
CCL22	**<0.001**	0.219	**<0.001**	0.602	**0.018**	**<0.001**	1.000
CCL3	**<0.001**	**<0.001**	**<0.001**	0.141	**0.025**	0.620	**0.028**
CCL4	**<0.001**	**<0.001**	**<0.001**	0.123	0.138	**<0.001**	0.073
sCD25/ sIL-2Rα	**<0.001**	**<0.001**	**<0.001**	0.190	0.838	**<0.001**	0.224
sFASLG	**<0.001**	0.092	**<0.001**	0.668	**0.010**	**<0.001**	0.149
sL-Selectin	0.744	0.062	0.157	0.128	0.101	**<0.001**	**<0.001**
IL-1RA	**<0.001**	0.435	**<0.001**	0.097	**0.025**	**0.009**	**0.046**
IL-18	0.155	**0.011**	**<0.001**	0.384	NA	**0.010**	NA
sVEGFR1	**<0.001**	**<0.001**	0.463	0.685	0.305	0.051	**<0.001**
sTNFRII	**<0.001**	**0.002**	**<0.001**	0.141	0.086	**<0.001**	**0.025**
sTNFRI	**<0.001**	**<0.001**	**<0.001**	0.134	**0.038**	0.537	**0.042**
LBP	**<0.001**	0.063	**<0.001**	0.171	**0.016**	**0.009**	**0.005**
MMP-9	**<0.001**	0.418	**<0.001**	0.880	**0.001**	**<0.001**	**0.002**
Ferritin	**0.0E0**	**<0.001**	**<0.001**	0.134	**<0.001**	**<0.001**	0.079
Lactoferrin	**<0.001**	0.708	**0.001**	0.112	**0.014**	**<0.001**	0.229
MPO	**<0.001**	**<0.001**	**<0.001**	0.128	**<0.001**	**<0.001**	0.492
IFN-α2a	**0.028**	**<0.001**	**<0.001**	0.371	0.897	**0.002**	0.073
IFN-γ	**<0.001**	**<0.001**	**0.002**	0.618	0.838	0.901	0.516
IL-10	**<0.001**	**<0.001**	**<0.001**	0.825	0.424	0.216	0.540
IL-12p70	0.308	**0.009**	**0.007**	0.246	0.239	**<0.001**	**<0.001**
IL-2	**<0.001**	0.418	**<0.001**	0.310	0.832	**0.009**	**0.005**
TNF-α	**<0.001**	**0.011**	**<0.001**	0.214	**0.042**	**<0.001**	0.160
GM-CSF	0.088	0.584	0.233	0.844	0.342	**<0.001**	0.305
IL-5	**0.003**	0.164	**0.029**	0.198	0.696	**<0.001**	0.156
sICAM-1	**0.008**	**0.035**	**<0.001**	0.702	0.255	**<0.001**	**0.005**
IL-3	0.113	0.080	0.744	0.269	NA	0.166	NA
IL-33	**<0.001**	**<0.001**	**<0.001**	0.501	**<0.001**	**<0.001**	**<0.001**
RAGE	**<0.001**	0.223	**<0.001**	0.570	0.403	**<0.001**	0.446
sVCAM-1	**<0.001**	**<0.001**	**<0.001**	0.335	0.323	**<0.001**	0.868
sCD163	**0.005**	**0.038**	**<0.001**	0.539	0.067	0.349	0.119
CXCL9	**<0.001**	**<0.001**	**<0.001**	0.501	0.390	**<0.001**	**<0.001**
G-CSF	**0.005**	**0.026**	0.198	0.684	0.228	0.064	**<0.001**

Author Manuscript Author Manuscript Author Manuscript Author Manuscript

Biomarker	MIS-C (n=48) vs pHC (n=53)	pCOVID-19 (n=57) vs pHC (n=53)	MIS-C (n=48) vs pCOVID-19 (n=57)	Mild (n=45) vs moderate (n=9) pCOVID-19	Moderate COVID-19 in adults (n=26) vs children (n=9)	Adult (n=45) vs pediatric (n=53) HC	Moderate COVID-19 in adults (n=26) vs children (n=9), adjusted for baseline differences in healthy adults and children
M-CSF	**<0.001**	**<0.001**	0.388	0.205	0.939	**<0.001**	0.565
Reg3A	**<0.001**	0.809	**<0.001**	0.372	**0.002**	0.058	**<0.001**
sST2/ sIL-33R	**0.0E0**	**0.008**	**<0.001**	0.384	0.643	**0.001**	**0.016**
sE-Selectin	**<0.001**	**0.011**	**<0.001**	0.685	**0.005**	**<0.001**	0.110
CX3CL1	**<0.001**	0.118	**<0.001**	0.954	**<0.001**	**<0.001**	**0.008**
TNFSF14	**<0.001**	**<0.001**	0.442	0.112	**0.002**	**<0.001**	0.522
SCF	0.123	**0.013**	**<0.001**	0.618	0.616	**0.027**	1.000

aHC: adult heathy controls; HC, healthy controls; MIS-C, multisystem inflammatory syndrome in children; pCOVID-19, pediatric COVID-19; pHC, pediatric healthy controls Analysis performed with Mann-Whitney U test with two-sided P values on results obtained within the first 7 days since onset of symptoms (for acute COVID) or hospitalization (for MIS-C). P values indicating statistical significance are shown. Bold formatting indicates statistically significant differences..

Extended Data Table 2 -

Biomarkers with significantly different concentrations in the first 7 days of illness (for pCOVID-19) or hospitalization (for MIS-C) by multivariate analysis adjusted for gender, age and ethnicity.

pCOVID-19 (n=57) vs pHC (n=52)				
Biomarker	**Median in pCOVID-19**	**Median in pHC**	**OR**	**95% CI**
IL-33	5.94	14.97	0.513	0.395–0.667***
MIS-C (n=46) vs pHC (n=52)				
Biomarker	**Median in MIS-C**	**Median in pHC**	**OR**	**95% CI**
CCL22	711	2100	0.995	0.992–0.998**
CCL3	64.3	24.1	1.255	1.085–1.452**
pCOVID-19 (n=57) vs MIS-C (n=46)				
Biomarker	**Median in pCOVID-19**	**Median in MIS-C**	**OR**	**95% CI**
IL-15	2.1	4.4	0.513	0.353–0.747***
CCL22	1856	711	1.002	1.001–1.003***

A standard multiple regression analysis was performed on subjects for whom there were no missing values for biomarkers (MIS-C: 46/48; pCOVID-19: 57/57; pHC: 52/53). Two-sided p values are marked as follows:

*
<0.05

**
<0.01

***
<0.001.

CI, confidence intervals; MIS-C, multisystem inflammatory syndrome in children; pCOVID-19, children with acute COVID-19; pHC, pediatric healthy controls.

Author Manuscript Author Manuscript Author Manuscript Author Manuscript

Extended Data Table 3 -

HLA allele composition in Italian patients with MIS-C compared to children with COVID-19 and healthy children

Category	Subject #	Predicted Ancestry	HLA class I			HLA Class II						
			A	B	C	DQA1	DQB1	DRB1	DPA1	DPB1	DRB3	DRB4
MIS-C	TO-006	EUR	*02, *11	*35; *52	*04; *12	*01; *05	*05; *03	*01; *11	*01; *01	*04; *04	*02; *02	*03; *03
	TO-009	EUR	*02, *02	*35; *37	*04; *06	*01; *04	*04; *06	*08; *15	*01; *01	*04; *04	*01; *01	*03; *03
	TO-010	EUR	*02; *H	*35; *53	*04; *04	*01; *05	*03; *05	*11; *14	*01; *01	*04; *04	*02; *02	*03; *03
	TO-017	EUR	*02; *24	*35; *35	*04; *04	*01; *05	*03; *05	*11; *14	*01; *01	*04; *10	*02; *02	*03; *03
	PV-006	EUR	*02; *68	*35; *35	*04; *04	*01; *03	*03; *05	*08; *14	*01; *01	*04; *13	*02; *02	*03; *03
	PV-009	EUR	*32; *24	*38; *55	*03; *12	*03; *05	*03; *03	*04; *11	*01; *01	*04; *04	*02; *02	*01; *03
	TO-001	EUR	*29; *30	*44; *53	*04; *16	*03; *04	*03; *04	*08; *13	*01; *01	*03; *04	*03; *03	*03; *03
	TO-024	AFR	*23; *36	*53; *58	*03; *04	*01; *02	*02; *06	*07; *13	*02; *03	*01; *04	*03; *03	*01; *03
	TO-027	AFR	*02; *30	*44; *53	*04; *07	*02; *05	*02; *02	*03; *13	*02; *02	*01; *17	*02; *02	*03; *03
Healthy	PV-173	EUR	*03; *68	*18; *51	*12; *14	*05; *06	*03; *03	*08; *11	*01; *01	*02; *03	*02; *02	*03; *03
	PV-172	EUR	*01; *03	*08; *35	*04; *07	*05; *05	*02; *02	*03; *03	*01; *01	*02; *14	*01; *02	*03; *03
	PV-171	EUR	*01; *03	*08; *35	*04; *07	*05; *05	*02; *02	*03; *03	*02; *02	*01; *14	*01; *02	*03; *03
	PV-170	EUR	*24; *68	*18; *52	*05; *12	*01; *05	*02; *06	*03; *15	*01; *02	*13; *13	*02; *02	*03; *03
	PV-167	EUR	*03; *24	*44; *55	*03; *05	*01; *01	*05; *05	*01; *16	*01; *01	*04; *04	*01; *01	*03; *03
	PV-165	EUR	*01; *11	*35; *38	*04; *12	*01; *05	*03; *06	*11; *15	*01; *01	*02; *15	*02; *02	*03; *03
	PV-162	EUR	*24; *26	*18; *40	*05; *07	*01; *05	*02; *05	*01; *03	*01; *02	*04; *10	*01; *01	*03; *03
	PV-161	EUR	*01; *02	*18; *44	*05; *07	*01; *02	*02; *05	*07; *15	*01; *02	*02; *14	*01; *01	*01; *03
	PV-160	EUR	*02; *03	*44; *57	*05; *18	*01; *02	*02; *06	*07; *15	*01; *01	*02; *04	*01; *01	*01; *03
	PV-159	EUR	*01; *03	*38; *57	*12; *18	*01; *01	*05; *06	*10; *15	*01; *01	*04; *13	*01; *01	*03; *03
	PV-150	EUR	*01; *24	*35; *51	*01; *15	*03; *03	*03; *03	*04; *04	*02; *02	*13; *14	*01; *01	*01; *01
	PV-149	EUR	*02; *11	*15; *18	*01; *12	*01; *03	*03; *05	*09; *15	*01; *01	*02; *04	*01; *01	*01; *03
	PV-148	EUR	*01; *25	*08; *08	*07; *07	*01; *05	*03; *06	*11; *13	*01; *01	*02; *04	*01; *02	*03; *03
	PV-142	EUR	*03; *24	*18; *35	*04; *12	*03; *05	*03; *03	*04; *11	*01; *01	*04; *04	*02; *02	*01; *03

Author Manuscript Author Manuscript Author Manuscript Author Manuscript

pCOVID-19	PV-140	EUR	*02; *32	*40; *50	*03; *06	*02; *02	*02; *03	*07; *15	*02; *02	*13; *14	*01; *01	*01; *01
	PV-139	EUR	*02; *32	*40; *50	*03; *06	*02; *02	*02; *03	*07; *15	*02; *02	*13; *14	*01; *01	*01; *01
	PV-138	EUR	*02; *30	*07; *13	*06; *07	*01; *02	*02; *06	*07; *15	*01; *01	*04; *04	*01; *01	*01; *03
	PV-137	EUR	*02; *30	*07; *13	*06; *07	*01; *02	*02; *06	*07; *15	*01; *01	*04; *04	*01; *01	*01; *03
	PV-136	EUR	*33; *11	*14; *35	*04; *08	*01; *01	*05; *05	*01; *16	*01; *02	*04; *10	*01; *01	*03; *03
	PV-134	EUR	*24; *32	*13; *44	*04; *06	*02; *05	*02; *02	*03; *07	*01; *01	*04; *04	*01; *01	*01; *03
	TO-023	EUR	*24; *24	*35; *49	*04; *07	*03; *05	*03; *03	*04; *11	*01; *01	*03; *04	*02; *02	*01; *03
	TO-022	EUR	*32; *24	*07; *49	*07; *07	*01; *03	*03; *05	*04; *16	*01; *01	*02; *04	*01; *01	*01; *03
	TO-021	EUR	*32; *24	*07; *49	*07; *07	*01; *03	*03; *05	*04; *16	*01; *01	*02; *04	*01; *01	*01; *03
	TO-020	EUR	*01; *32	*44; *57	*05; *06	*02; *05	*03; *03	*07; *11	*01; *01	*02; *04	*02; *02	*01; *03
	TO-019	EUR	*11; *24	*39; *51	*12; *15	*01; *05	*03; *05	*11; *16	*02; *02	*14; *17	*02; *02	*03; *03
	TO-018	EUR	*01; *03	*37; *49	*07; *06	*01; *05	*03; *06	*11; *13	*01; *01	*02; *04	*02; *03	*03; *03
	PV-123	EUR	*24; *69	*13; *55	*03; *06	*01; *02	*02; *05	*07; *14	*02; *02	*17; *17	*02; *02	*01; *03
	BS-HS-235	EUR	*02; *30	*13; *13	*06; *06	*02; *02	*02; *02	*07; *15	*01; *01	*04; *04	*01; *01	*01; *01
	TO-016	EUR	*26; *68	*38; *40	*02; *12	*01; *05	*03; *06	*11; *13	*01; *01	*02; *04	*01; *02	*03; *03
	TO-014	EUR	*24; *25	*40; *44	*05; *15	*01; *05	*03; *05	*11; *14	*01; *01	*04; *04	*02; *02	*03; *03
	TO-013	EUR	*32; *68	*18; *57	*07; *12	*01; *02	*02; *05	*07; *14	*01; *02	*02; *10	*02; *02	*01; *03
	TO-012	EUR	*03; *03	*07; *35	*04; *07	*01; *01	*05; *05	*01; *14	*01; *02	*04; *05	*02; *02	*03; *03
	TO-011	EUR	*32; *68	*18; *57	*07; *12	*01; *02	*02; *05	*07; *14	*01; *02	*02; *10	*02; *02	*01; *03
	TO-008	EUR	*23; *68	*35; *49	*07; *07	*04; *05	*03; *04	*08; *12	*01; *01	*04; *04	*02; *02	*03; *03
	TO-007	EUR	*02; *03	*49; *73	*07; *15	*01; *03	*02; *05	*01; *04	*01; *01	*03; *13	*01; *01	*01; *01
	TO-005	EUR	*02; *24	*08; *18	*07; *12	*01; *05	*03; *05	*01; *11	*01; *02	*02; *04	*02; *02	*03; *03
	TO-004	EUR	*02; *23	*41; *44	*04; *17	*01; *02	*02; *06	*07; *13	*01; *01	*02; *02	*03; *03	*01; *03
	TO-003	EUR	*26; *01	*15; *18	*03; *06	*01; *05	*03; *05	*11; *16	*01; *01	*02; *02	*02; *02	*03; *03
	TO-002	EUR	*02; *32	*15; *44	*02; *07	*01; *01	*05; *06	*13; *16	*01; *01	*02; *04	*03; *03	*03; *03
	PV-031	EUR	*02; *26	*39; *52	*12; *12	*01; *05	*03; *06	*11; *15	*01; *01	*02; *04	*02; *02	*03; *03
	PV-015	EUR	*26; *32	*38; *51	*02; *12	*01; *01	*05; *05	*01; *16	*01; *01	*04; *10	*01; *01	*03; *03

Author Manuscript Author Manuscript Author Manuscript Author Manuscript

PV-008	EUR	*03; *11	*35; *49	*04; *07	*01; *02	*02; *05	*07; *15	*01; *01	*01; *04	*01; *01	*01; *03
PV-007	EUR	*03; *24	*51; *57	*07; *15	*02; *05	*03; *03	*07; *11	*01; *01	*03; *04	*02; *02	*01; *03
PV-002	EUR	*02; *02	*08; *15	*03; *07	*01; *05	*02; *05	*03; *14	*01; *01	*03; *14	*02; *02	*03; *03
CG-807	EUR	*01; *02	*08; *50	*06; *07	*02; *05	*02; *02	*03; *07	*01; *01	*04; *04	*01; *01	*01; *03
PV-156	AMR	*02; *24	*39; *40	*07; *08	*04; *04	*03; *04	*08; *08	*01; *01	*04; *04	*01; *01	*01; *01
PV-154	AMR	*02; *24	*39; *40	*07; *08	*04; *04	*03; *04	*08; *08	*01; *01	*04; *04	*01; *01	*01; *01
PV-152	AMR	*01; *24	*35; *51	*01; *15	*03; *03	*03; *03	*04; *04	*02; *02	*13; *14	*01; *01	*01; *01
PV-144	AMR	*01; *26	*15; *40	*02; *15	*03; *05	*03; *03	*04; *11	*01; *01	*03; *04	*02; *02	*03; *03
PV-133	AMR	*01; *32	*50; *58	*07; *17	*02; *05	*02; *02	*03; *07	*01; *02	*03; *17	*01; *01	*01; *03
PV-132	AMR	*32; *01	*50; *58	*17; *07	*02; *05	*02; *02	*03; *07	*01; *02	*03; *17	*01; *01	*01; *03
PV-130	AMR	*24; *29	*45; *45	*06; *16	*01; *02	*02; *05	*07; *10	*01; *01	*04; *17	*01; *01	*01; *03
PV-129	AMR	*24; *29	*45; *45	*06; *16	*01; *02	*02; *05	*07; *10	*01; *01	*04; *17	*01; *01	*01; *03
PV-087	AMR	*02; *34	*27; *35	*02; *06	*01; *01	*05; *06	*13; *16	*01; *01	*04:*85	*02; *02	*03; *03
TO-015	AMR	*02; *24	*44; *51	*05; *15	*01; *03	*03; *06	*09; *13	*01; *02	*04; *05	*03; *03	*01; *03
PV-005	AMR	*26; *36	*14; *15	*02; *08	*02; *02	*02; *02	*07; *07	*01; *02	*04; *11	*01; *01	*01; *01
PV-164	AFR	*03; *03	*15; *42	*14; *17	*02; *05	*02; *02	*03; *07	*02; *02	*01; *01	*02; *02	*01; *03
PV-127	AFR	*03; *03	*53; *53	*04; *04	*01; *04	*03; *06	*08; *11	*02; *02	*01; *01	*03; *03	*03; *03
PV-126	AFR	*02; *30	*15; *18	*14; *18	*01; *03	*02; *06	*09; *15	*01; *02	*01; *02	*01; *01	*01; *03
BS-NEW-49	AFR	*33; *68	*07; *44	*04; *15	*01; *01	*05; *05	*01; *11	*01; *03	*01; *04	*02; *02	*03; *03
PV-088	AFR	*02; *30	*07; *42	*07; *17	*01; *05	*02; *06	*03; *15	*02; *03	*01; *04	*02; *02	*03; *03
PV-158	SAS	*68; *32	*35; *35	*04; *07	*01; *01	*05; *06	*13; *14	*02; *02	*13; *17	*01; *02	*03; *03
PV-157	SAS	*24; *33	*58; *58	*03; *03	*03; *05	*02; *03	*03; *04	*01; *02	*02; *04	*02; *02	*01; *03
PV-131	SAS	*68; *02	*37; *51	*06; *16	*01; *01	*05; *05	*10; *10	*01; *01	*02; *04	*01; *01	*03; *03
CT-057	EUR	*01; *02	*15; *35	*03; *04	*02; *05	*03; *03	*07; *11	*01; *02	*04; *13	*02; *02	*01; *03
CT-014	EUR	*02; *24	*18; *35	*04; *07	*03; *05	*03; *03	*04; *11	*01; *01	*02; *04	*02; *02	*01; *03
CT-056	EUR	*01; *03	*15; *44	*07; *16	*01; *05	*03; *06	*11; *13	*01; *01	*09; *264	*02; *03	*03; *03
CT-055	EUR	*01; *03	*49; *51	*07; *15	*01; *01	*05; *06	*13; *16	*01; *01	*04; *04	*03; *03	*03; *03

Author Manuscript Author Manuscript Author Manuscript Author Manuscript

	CT-053	EUR	*01; *03	*35; *49	*07; *12	*01; *05	*03; *05	*11; *14	*01; *01	*02; *03	*02; *02	*03; *03
	CT-052	EUR	*01; *01	*40; *57	*06; *15	*01; *01	*05; *05	*01; *14	*01; *02	*04; *17	*02; *02	*03; *03
	CT-050	EUR	*01; *02	*08; *18	*07; *07	*01; *05	*02; *05	*01; *03	*01; *01	*02; *04	*02; *02	*03; *03
	CT-049	EUR	*24; *32	*18; *38	*07; *12	*01; *05	*03; *06	*11; *13	*01; *01	*02; *04	*01; *02	*03; *03
	CT-048	EUR	*03; *03	*18; *40	*12; *12	*01; *02	*02; *05	*01; *07	*01; *01	*04; *04	*01; *01	*01; *01
	CT-045	EUR	*02; *31	*39; *51	*12; *15	*01; *05	*02; *06	*03; *13	*01; *02	*01; *03	*01; *02	*03; *03
	CT-044	EUR	*24; *24	*18; *41	*07; *07	*01; *05	*03; *06	*11; *15	*01; *01	*04; *13	*02; *02	*03; *03
	CT-043	EUR	*03; *68	*07; *38	*12; *15	*01; *03	*03; *06	*04; *13	*01; *01	*03; *04	*01; *01	*01; *03
	CT-041	EUR	*02; *23	*18; *41	*12; *17	*01; *05	*03; *06	*11; *13	*01; *02	*04; *11	*01; *02	*03; *03
	CT-038	EUR	*02; *24	*13; *45	*06; *16	*01; *05	*03; *05	*10; *12	*01; *03	*04; *04	*02; *02	*03; *03
	CT-037	EUR	*24; *31	*27; *44	*02; *02	*01; *05	*03; *06	*11; *13	*01; *02	*04; *10	*01; *02	*03; *03
	CT-034	EUR	*02; *02	*45; *51	*14; *16	*01; *04	*04; *05	*08; *11	*01; *01	*04; *04	*03; *03	*03; *03
	CT-033	EUR	*02; *11	*18; *27	*01; *12	*05; *05	*03; *03	*11; *11	*01; *01	*04; *04	*02; *02	*03; *03
	CT-028	EUR	*32; *32	*15; *57	*07; *12	*01; *02	*02; *06	*07; *13	*01; *01	*02; *02	*03; *03	*01; *03
	CT-025	EUR	*03; *23	*49; *51	*07; *14	*05; *06	*03; *03	*08; *11	*01; *01	*03; *04	*02; *02	*03; *03
	CT-024	EUR	*01; *23	*39; *40	*02; *12	*01; *05	*03; *06	*11; *13	*01; *01	*04; *04	*02; *02	*03; *03
	CT-022	EUR	*01; *24	*08; *51	*07; *15	*01; *05	*02; *06	*03; *13	*01; *01	*02; *02	*01; *03	*03; *03
pHC	CT-021	EUR	*03; *23	*18; *39	*12; *12	*01; *01	*05; *06	*13; *16	*01; *02	*01; *04	*02; *02	*03; *03
	CT-017	EUR	*01; *23	*13; *44	*04; *06	*02; *02	*02; *02	*07; *15	*02; *02	*05; *17	*01; *01	*01; *01
	CT-016	EUR	*23; *29	*44; *49	*07; *16	*02; *05	*02; *03	*07; *11	*01; *01	*01; *02	*02; *02	*01; *03
	CT-015	EUR	*02; *26	*51; *51	*01; *05	*01; *05	*03; *06	*11; *13	*01; *01	*02; *04	*01; *02	*03; *03
	CT-013	EUR	*02; *26	*18; *44	*05; *14	*01; *05	*02; *06	*03; *15	*01; *01	*04; *04	*02; *02	*03; *03
	CT-012	EUR	*02; *11	*44; *57	*05; *06	*01; *02	*03; *05	*07; *11	*01; *01	*02; *04	*02; *02	*01; *03
	CT-011	EUR	*11; *25	*18; *53	*04; *12	*01; *01	*05; *06	*01; *13	*02; *02	*03; *10	*03; *03	*03; *03
	CT-010	EUR	*02; *02	*15; *18	*12; *12	*02; *05	*02; *03	*07; *11	*01; *01	*02; *04	*02; *02	*01; *03
	CT-009	EUR	*11; *25	*18; *53	*04; *12	*01; *01	*05; *06	*01; *13	*02; *02	*03; *10	*03; *03	*03; *03
	CT-008	EUR	*02; *24	*18; *51	*01; *12	*05; *05	*03; *03	*11; *11	*01; *01	*04; *04	*02; *02	*03; *03

Author Manuscript Author Manuscript Author Manuscript Author Manuscript

CT-004	EUR	*03; *33	*14; *27	*02; *08	*01; *01	*05; *06	*01; *13	*01; *01	*02; *04	*01; *01	*03; *03
CT-003	EUR	*03; *33	*14; *35	*04; *08	*01; *02	*02; *05	*01; *07	*01; *01	*04; *04	*01; *01	*01; *03
CT-002	EUR	*01; *24	*15; *51	*03; *16	*01; *05	*03; *06	*11; *13	*01; *01	*04; *13	*02; *03	*03; *03
CT-001	EUR	*01; *02	*13; *51	*06; *14	*02; *05	*02; *03	*07; *11	*01; *01	*04; *04	*02; *02	*01; *03
CT-054	SAS	*03; *24	*44; *48	*07; *08	*02; *05	*02; *03	*07; *11	*01; *01	*02; *03	*02; *02	*01; *03
CT-039	SAS	*11; *11	*15; *51	*07; *15	*01; *03	*03; *06	*04; *13	*01; *01	*02; *04	*03; *03	*01; *03
CT-030	SAS	*03; *33	*44; *44	*07; *07	*02; *06	*02; *03	*07; *12	*01; *02	*02; *269	*03; *03	*01; *01
CT-051	AFR	*11; *26	*08; *55	*03; *07	*01; *05	*03; *05	*11; *14	*01; *01	*01; *04	*02; *02	*03; *03
CT-026	EAS	*33; *34	*40; *44	*07; *12	*01; *02	*02; *05	*07; *15	*02; *02	*01; *01	*01; *01	*01; *03
CT-036	AMR	*02; *29	*13; *15	*01; *06	*01; *03	*03; *06	*09; *13	*01; *01	*04; *04	*02; *02	*01; *03
CT-032	AMR	*02; *24	*07; *07	*07; *15	*04; *05	*03; *04	*08; *11	*01; *01	*02; *04	*02; *02	*03; *03
CT-027	AMR	*03; *32	*35; *40	*02; *04	*01; *03	*03; *06	*04; *13	*01; *01	*02; *04	*03; *03	*01; *03
CT-018	AMR	*02; *30	*18; *42	*05; *17	*04; *05	*02; *04	*03; *03	*01; *03	*04; *04	*01; *02	*03; *03

Association with HLA-A*02, B*35, C*04 alleles^ (Fisher's exact t test)	
	p value
MIS-C vs. pCOVID-19	<0.0001
MIS-C vs. pHC	0.0005
pCOVID-19 vs. pHC	NS

AFR, Africa; AMR, America; EAS: East Asia; EUR, Europe; MIS-C, multisystem inflammatory syndrome in children; pCOVID-19, pediatric COVID-19; pHC, pediatric healthy controls; SAS, South Asia..

The HLA-A*02, B*35 and C*04 alleles, and subjects sharing a combination of all three these alleles are highlighted in red..

^Analysis performed on subjects of European ancestry only

Supplementary Material

Refer to Web version on PubMed Central for supplementary material.

Authors

Keith Sacco[1,*], Riccardo Castagnoli[1,2,*], Svetlana Vakkilainen[1,*], Can Liu[3,*], Ottavia M. Delmonte[1], Cihan Oguz[4], Ian M. Kaplan[5], Sara Alehashemi[1], Peter D. Burbelo[6], Farzana Bhuyan, Adriana A. de Jesus[1,1], Kerry Dobbs[1], Lindsey B. Rosen[1], Aristine Cheng[1], Elana Shaw[1], Mikko S. Vakkilainen[7], Francesca Pala[1], Justin Lack[4], Yu

Author Manuscript Author Manuscript Author Manuscript Author Manuscript

Zhang[1], Danielle L Fink[8], Vasileios Oikonomou, Andrew L. Snow[1,9], Clifton L. Dalgard[10,11], Jinguo Chen[12], Brian A. Sellers[12], Gina A. Montealegre Sanchez[13], Karyl Barron[14], Emma Rey-Jurado[15], Cecilia Vial[15], Maria Cecilia Poli[15,16], Amelia Licari[2], Daniela Montagna[2,17], Gian Luigi Marseglia[2], Francesco Licciardi[18], Ugo Ramenghi[18], Valentina Discepolo[19], Andrea Lo Vecchio[19], Alfredo Guarino[19], Eli M. Eisenstein[20], Luisa Imberti[21], Alessandra Sottini[21], Andrea Biondi[22], Sayonara Mató[23], Dana Gerstbacher[24], Meng Truong[1], Michael A. Stack[1], Mary Magliocco[25], Marita Bosticardo[1], Tomoki Kawai[1], Jeffrey J. Danielson[1], Tyler Hulett[26], Manor Askenazi[26], Shaohui Hu[26], NIAID Immune Response to COVID Group[†], Chile MIS-C Group[†], Pavia Pediatric COVID-19 Group[†], Jeffrey I. Cohen[27], Helen C. Su[1], Douglas B. Kuhns[8], Michail S. Lionakis[1], Thomas M. Snyder[5], Steven M. Holland[1], Raphaela Goldbach-Mansky[1], John S. Tsang[28], Luigi D. Notarangelo[1,#]

Affiliations

[1]Laboratory of Clinical Immunology and Microbiology, National Institute of Allergy and Infectious Diseases, National Institutes of Health, Bethesda, MD 20892, USA

[2]Pediatric Clinic, Fondazione IRCCS Policlinico San Matteo, Pavia, Italy; Department of Clinical, Surgical, Diagnostic and Pediatric Sciences, University of Pavia, Pavia, Italy

[3]Multiscale Systems Biology Section, Laboratory of Immune System Biology, NIAID, NIH, Bethesda, MD 20892, USA; Graduate Program in Biological Sciences, University of Maryland, College Park, MD 20742, USA

[4]NIAID Collaborative Bioinformatics Resource (NCBR), National Institute of Allergy and Infectious Diseases, National Institutes of Health, Bethesda, MD 20892, USA; Advanced Biomedical Computational Science, Frederick National Laboratory for Cancer Research, Leidos Biomedical Research, Inc., Frederick, MD 21702, USA

[5]Adaptive Biotechnologies, Seattle, WA 98109, USA

[6]National Institute of Dental and Craniofacial Research, National Institutes of Health, Bethesda, MD 20892, USA

[7]Department of Computer Science, Aalto University, Helsinki, Finland

[8]Applied/Developmental Research Directorate, Frederick National Laboratory for Cancer Research, Frederick, MD 21702, USA

[9]Department of Pharmacology & Molecular Therapeutics, Uniformed Services, University of the Health Sciences, Bethesda, MD 20892, USA

[10]Department of Anatomy, Physiology & Genetics, Uniformed Services University of the Health Sciences, Bethesda, MD 20814

[11]The American Genome Center, Uniformed Services University of the Health Sciences, Bethesda, MD 20815, USA

[12]Trans-NIH Center for Human Immunology, Autoimmunity, and Inflammation (CHI), National Institutes of Health, Bethesda, MD 20892, USA

Author Manuscript Author Manuscript Author Manuscript Author Manuscript

[13]Intramural Clinical Management and Operation Branch (ICMOB), Division of Clinical Research, National Institute of Allergy and Infectious Diseases, National Institutes of Health, Bethesda, MD 20892, USA

[14]Division of Intramural Research, National Institute of Allergy and Infectious Diseases, National Institutes of Health, Bethesda, MD 20892, USA

[15]Facultad de Medicina Clínica Alemana Universidad del Desarrollo, Santiago, Chile

[16]Unidad de Inmunología y Reumatología, Hospital de niños Dr. Roberto del Río, Santiago, Chile

[17]Laboratory of Immunology and Transplantation, Fondazione IRCCS Policlinico San Matteo, Pavia, Italy

[18]Department of Pediatric and Public Health Sciences, Regina Margherita Children's Hospital, A.O.U. Città Della Salute E Della Scienza Di Torino, University of Turin, Turin, Italy

[19]Department of Translational Medical Sciences, Section of Pediatrics, University of Naples Federico II, Napoli, Italy

[20]Department of Pediatrics, Hadassah-Hebrew University Medical Center, Mount Scopus, Jerusalem, Israel

[21]CREA Laboratory (AIL Center for Hemato-Oncologic Research), Diagnostic Department, ASST Spedali Civili di Brescia, Brescia, Italy

[22]Pediatric Department and Centro Tettamanti-European Reference Network PaedCan, EuroBloodNet, MetabERN-University of Milano-Bicocca-Fondazione MBBM- Ospedale San Gerardo, Monza, Italy

[23]Randall Children's Hospital at Legacy Emanuel, Portland, Oregon, OR 97227, USA

[24]Division of pediatric Rheumatology, Stanford Children's Hospital, Stanford, CA 94304, USA

[25]Molecular Development of the Immune System Section, Laboratory of Immune System Biology, NIAID, NIH, Bethesda, MD 20892, USA

[26]CDI Laboratories, Antygen Division, Baltimore, MD 21205, USA

[27]Laboratory of Infectious Diseases, National Institute of Allergy and Infectious diseases, National Institutes of Health, Bethesda, MD 20892, USA

[28]Multiscale Systems Biology Section, Laboratory of Immune System Biology, NIAID, NIH, Bethesda, MD 20892, USA; NIH Center for Human Immunology, NIAID, NIH, Bethesda, MD 20892, USA

Acknowledgements

We thank the patients, their families, and healthy donors for placing their trust in us.

Author Manuscript Author Manuscript Author Manuscript Author Manuscript

We thank Andrea Catzola, MD, and Luca Pierri, MD, from the Pediatric COVID19 HUB at the University of Naples Federico II, and Evelyn Nuñez, from the Unidad de Inmunología y Reumatología, Hospital de niños Dr. Roberto del Río, for helping with consenting patients and samples collection, without any compensation.

We thank CDI Antygen HuProt Division (Baltimore, MD and Mayaguez, PR), and in particular Shuang Liu, Bradley Moore, Pedro Ramos and Oscar Candelario for *HuProt™* Autoantibody analysis.

This work was supported by the Division of Intramural Research, National Institute of Allergy and Infectious Diseases (grants ZIA AI001270-01 to LDN and ZIA AI001265 to HCS), National Institute of Dental and Craniofacial Research, National Institutes of Health, by Regione Lombardia, Italy (project "Risposta immune in pazienti con COVID-19 e co-morbidità" to RC, AL, DM, GLM for Pavia, Italy and to LI and AS for Brescia, Italy), by ANID COVID 0999 to CV and MCP, Fondecyt n° 1201240 to CV, Fondecyt n° 11181222 (to MCP, Chile). In addition, this project has been funded in part with federal funds from the National Cancer Institute, National Institutes of Health, under Contract No. 75N91019D00024 (to DBK).

The content of this publication does not necessarily reflect the views or policies of the Department of Health and Human Services, nor does mention of trade names, commercial products, or organizations imply endorsement by the U.S. Government. Moreover, the opinions and assertions expressed herein are those of the authors and are not to be construed as reflecting the views of Uniformed Services University of the Health Sciences or the United States Department of Defense.

RC is a participant in the USA National Institutes of Health (NIH) Graduate Partnership Program between NIH and the University of Pavia, Italy.

SV is funded by The Finnish Medical Foundation and Orion Research Foundation sr.

References

1. Castagnoli R, et al. Severe Acute Respiratory Syndrome Coronavirus 2 (SARS-CoV-2) Infection in Children and Adolescents: A Systematic Review. JAMA Pediatr 174, 882–889 (2020). [PubMed: 32320004]
2. Shekerdemian LS, et al. Characteristics and Outcomes of Children With Coronavirus Disease 2019 (COVID-19) Infection Admitted to US and Canadian Pediatric Intensive Care Units. JAMA Pediatr 174, 868–873 (2020). [PubMed: 32392288]
3. Verdoni L, et al. An outbreak of severe Kawasaki-like disease at the Italian epicentre of the SARS-CoV-2 epidemic: an observational cohort study. Lancet 395, 1771–1778 (2020). [PubMed: 32410760]
4. Riphagen S, Gomez X, Gonzalez-Martinez C, Wilkinson N & Theocharis P Hyperinflammatory shock in children during COVID-19 pandemic. Lancet 395, 1607–1608 (2020). [PubMed: 32386565]
5. CDC Health Advisory Panel. Multisystem Inflammatory Syndrome in Children (MIS-C) Associated with Coronavirus Disease 2019 (COVID-19). Centers for Disease Control and Prevention. Available at https://emergency.cdc.gov/han/2020/han00432.asp. Accessed 28 June 2021.
6. Williamson EJ, et al. Factors associated with COVID-19-related death using OpenSAFELY. Nature 584, 430–436 (2020). [PubMed: 32640463]
7. Zhang Q, et al. Inborn errors of type I IFN immunity in patients with life-threatening COVID-19. Science 370, eabd4570 (2020). [PubMed: 32972995]
8. Asano T, et al. X-linked recessive TLR7 deficiency in ~1% of men under 60 years old with life-threatening COVID-19. Sci Immunol 6, eabl4348 (2021). [PubMed: 34413140]
9. Bastard P, et al. Autoantibodies neutralizing type I IFNs are present in ~4% of uninfected individuals over 70 years old and account for ~20% of COVID-19 deaths. Sci Immunol 6, eabl4340 (2021). [PubMed: 34413139]
10. Pierce CA, et al. Immune responses to SARS-CoV-2 infection in hospitalized pediatric and adult patients. Sci Transl Med 12, eabd5487 (2020). [PubMed: 32958614]
11. Consiglio CR, et al. The Immunology of Multisystem Inflammatory Syndrome in Children with COVID-19. Cell 183, 968–981 e967 (2020). [PubMed: 32966765]

Author Manuscript Author Manuscript Author Manuscript Author Manuscript

12. Gruber CN, et al. Mapping Systemic Inflammation and Antibody Responses in Multisystem Inflammatory Syndrome in Children (MIS-C). Cell 183, 982–995 e914 (2020). [PubMed: 32991843]
13. Ramaswamy A, et al. Immune dysregulation and autoreactivity correlate with disease severity in SARS-CoV-2-associated multisystem inflammatory syndrome in children. Immunity 54, 1083–1095 e1087 (2021). [PubMed: 33891889]
14. Porritt RA, et al. The autoimmune signature of hyperinflammatory multisystem inflammatory syndrome in children. J Clin Invest 131, e15120 (2021).
15. Moreews M, et al. Polyclonal expansion of TCR Vbeta 21.3(+) CD4(+) and CD8(+) T cells is a hallmark of Multisystem Inflammatory Syndrome in Children. Sci Immunol 6, eabh1516 (2021). [PubMed: 34035116]
16. Esteve-Sole A, et al. Similarities and differences between the immunopathogenesis of COVID-19-related pediatric multisystem inflammatory syndrome and Kawasaki disease. J Clin Invest 131, e144554 (2021).
17. McArdle AJ, et al. Treatment of Multisystem Inflammatory Syndrome in Children. N Engl J Med 385, 11–22 (2021). [PubMed: 34133854]
18. DeBiasi RL Immunotherapy for MIS-C - IVIG, Glucocorticoids, and Biologics. N Engl J Med 385, 74–75 (2021). [PubMed: 34133878]
19. Abdel-Haq N, et al. SARS-CoV-2-associated multisystem inflammatory syndrome in children: clinical manifestations and the role of infliximab treatment. Eur J Pediatr 180, 1581–1591 (2021). [PubMed: 33452570]
20. Kim H, et al. Development of a Validated Interferon Score Using NanoString Technology. J Interferon Cytokine Res 38, 171–185 (2018). [PubMed: 29638206]
21. Abers MS, et al. An immune-based biomarker signature is associated with mortality in COVID-19 patients. JCI Insight 6, e144455 (2021).
22. Candia J, et al. Assessment of Variability in the SOMAscan Assay. Sci Rep 7, 14248 (2017). [PubMed: 29079756]
23. Fong JJ, et al. Siglec-7 engagement by GBS beta-protein suppresses pyroptotic cell death of natural killer cells. Proc Natl Acad Sci U S A 115, 10410–10415 (2018). [PubMed: 30254166]
24. Stoeckius M, et al. Simultaneous epitope and transcriptome measurement in single cells. Nat Methods 14, 865–868 (2017). [PubMed: 28759029]
25. Liu C, et al. Time-resolved systems immunology reveals a late juncture linked to fatal COVID-19. Cell 184, 1836–1857 e1822 (2021). [PubMed: 33713619]
26. Woods CW, et al. A host transcriptional signature for presymptomatic detection of infection in humans exposed to influenza H1N1 or H3N2. PLoS One 8, e52198 (2013). [PubMed: 23326326]
27. Querec TD et al. Systems biology approach predicts immunogenicity of the yellow fever vaccine in humans. Nat Immunol 10, 116–125 (2009). [PubMed: 19029902]
28. Yoshida M, et al. Local and systemic responses to SARS-CoV-2 infection in children and adults. Nature (2021).
29. Porritt RA, et al. HLA class I-associated expansion of TRBV11–2 T cells in multisystem inflammatory syndrome in children. J Clin Invest 131, e146614 (2021).
30. Hoste L, et al. TIM3+ TRBV11–2 T cells and IFNgamma signature in patrolling monocytes and CD16+ NK cells delineate MIS-C. J Exp Med 219, e20211381 (2022). [PubMed: 34914824]
31. McKinstry KK, Strutt TM & Swain SL Regulation of CD4+ T-cell contraction during pathogen challenge. Immunol Rev 236, 110–124 (2010). [PubMed: 20636812]
32. Herold MJ, McPherson KG & Reichardt HM Glucocorticoids in T cell apoptosis and function. Cell Mol Life Sci 63, 60–72 (2006). [PubMed: 16314919]
33. Swain SL, McKinstry KK & Strutt TM Expanding roles for CD4(+) T cells in immunity to viruses. Nat Rev Immunol 12, 136–148 (2012). [PubMed: 22266691]
34. Woodruff MC, et al. Extrafollicular B cell responses correlate with neutralizing antibodies and morbidity in COVID-19. Nat Immunol 21, 1506–1516 (2020). [PubMed: 33028979]

Author Manuscript Author Manuscript Author Manuscript Author Manuscript

35. Vella LA, et al. Deep immune profiling of MIS-C demonstrates marked but transient immune activation compared to adult and pediatric COVID-19. Sci Immunol 6, eabf7570 (2021). [PubMed: 33653907]
36. Durbin RK, Kotenko SV & Durbin JE Interferon induction and function at the mucosal surface. Immunol Rev 255, 25–39 (2013). [PubMed: 23947345]
37. Trouillet-Assant S, et al. Type I IFN immunoprofiling in COVID-19 patients. J Allergy Clin Immunol 146, 206–208 e202 (2020). [PubMed: 32360285]
38. Hadjadj J, et al. Impaired type I interferon activity and inflammatory responses in severe COVID-19 patients. Science 369, 718–724 (2020). [PubMed: 32661059]
39. Loske J, et al. Pre-activated antiviral innate immunity in the upper airways controls early SARS-CoV-2 infection in children. Nat Biotechnol (2021).
40. Brusilovsky M, et al. Environmental allergens trigger type 2 inflammation through ripoptosome activation. Nat Immunol 22, 1316–1326 (2021). [PubMed: 34531562]
41. Villarreal DO, et al. Molecular adjuvant IL-33 enhances the potency of a DNA vaccine in a lethal challenge model. Vaccine 33, 4313–4320 (2015). [PubMed: 25887087]
42. Chen Y & Qian J Increased serum levels of IL-33 and soluble ST2 in neonates with human cytomegalovirus infection. J Med Virol 90, 1383–1388 (2018). [PubMed: 29663450]
43. Zhang Y, et al. Comparative study of the cytokine/chemokine response in children with differing disease severity in enterovirus 71-induced hand, foot, and mouth disease. PLoS One 8, e67430 (2013). [PubMed: 23840697]
44. Jin HL, Zhan L, Mei SF & Shao ZY Serum Cytokines and FeNO in School-Aged Children with Mycoplasma pneumoniae Pneumonia. Med Sci Monit 26, e923449 (2020). [PubMed: 32564053]
45. Saravia J, et al. Respiratory Syncytial Virus Disease Is Mediated by Age-Variable IL-33. PLoS Pathog 11, e1005217 (2015). [PubMed: 26473724]
46. Rapp M, et al. CCL22 controls immunity by promoting regulatory T cell communication with dendritic cells in lymph nodes. J Exp Med 216, 1170–1181 (2019). [PubMed: 30910796]
47. Peine M, Marek RM & Lohning M IL-33 in T Cell Differentiation, Function, and Immune Homeostasis. Trends Immunol 37, 321–333 (2016). [PubMed: 27055914]
48. Yoshie O & Matsushima K CCR4 and its ligands: from bench to bedside. Int Immunol 27, 11–20 (2015). [PubMed: 25087232]
49. Kopach P, et al. IFN-gamma directly controls IL-33 protein level through a STAT1- and LMP2-dependent mechanism. J Biol Chem 289, 11829–11843 (2014). [PubMed: 24619410]
50. Yamashita U & Kuroda E Regulation of macrophage-derived chemokine (MDC, CCL22) production. Crit Rev Immunol 22, 105–114 (2002). [PubMed: 12433129]
51. Naba A, et al. The extracellular matrix: Tools and insights for the “omics” era. Matrix Biol 49, 10–24 (2016). [PubMed: 26163349]
52. Clarke LA, et al. Endothelial injury and repair in systemic vasculitis of the young. Arthritis Rheum 62, 1770–1780 (2010). [PubMed: 20178138]
53. Schulte-Schrepping J, et al. Severe COVID-19 Is Marked by a Dysregulated Myeloid Cell Compartment. Cell 182, 1419–1440 e1423 (2020). [PubMed: 32810438]
54. Reyes M, et al. Plasma from patients with bacterial sepsis or severe COVID-19 induces suppressive myeloid cell production from hematopoietic progenitors in vitro. Sci Transl Med 13, eabe9599 (2021). [PubMed: 34103408]
55. Yonker LM, et al. Multisystem inflammatory syndrome in children is driven by zonulin-dependent loss of gut mucosal barrier. J Clin Invest 131, e149633 (2021).
56. Loyal L, et al. Cross-reactive CD4(+) T cells enhance SARS-CoV-2 immune responses upon infection and vaccination. Science 374, eabh1823 (2021). [PubMed: 34465633]
57. Dowell AC, et al. Children develop robust and sustained cross-reactive spike-specific immune responses to SARS-CoV-2 infection. Nat Immunol 23, 40–49 (2022). [PubMed: 34937928]
58. Cheng MH, et al. Superantigenic character of an insert unique to SARS-CoV-2 spike supported by skewed TCR repertoire in patients with hyperinflammation. Proc Natl Acad Sci U S A 117, 25254–25262 (2020). [PubMed: 32989130]

Author Manuscript Author Manuscript Author Manuscript Author Manuscript

59. Kokkinopoulou I & Moutsatsou P Mitochondrial Glucocorticoid Receptors and Their Actions. Int J Mol Sci 22(2021).
60. Lanza L, et al. Prednisone increases apoptosis in in vitro activated human peripheral blood T lymphocytes. Clin Exp Immunol 103, 482–490 (1996). [PubMed: 8608650]
61. Brunetti M, et al. Spontaneous and glucocorticoid-induced apoptosis in human mature T lymphocytes. Blood 86, 4199–4205 (1995). [PubMed: 7492778]
62. Burbelo PD, et al. Autoantibodies Detected in MIS-C Patients due to Administration of Intravenous Immunoglobulin. medRxiv, 2021.2011.2003.21265769 (2021).

Methods-only References

63. COVID-19 Treatment Guidelines Panel. Coronavirus Disease 2019 (COVID-19) Treatment Guidelines. National Institutes of Health. Available at https://www.covid19treatmentguidelines.nih.gov/. Accessed 28 June 2021.
64. Burbelo PD, et al. Sensitivity in Detection of Antibodies to Nucleocapsid and Spike Proteins of Severe Acute Respiratory Syndrome Coronavirus 2 in Patients With Coronavirus Disease 2019. J Infect Dis 222, 206–213 (2020). [PubMed: 32427334]
65. Liu SY, Sanchez DJ, Aliyari R, Lu S & Cheng G Systematic identification of type I and type II interferon-induced antiviral factors. Proc Natl Acad Sci U S A 109, 4239–4244 (2012). [PubMed: 22371602]
66. Webtool For Basic Data Plotting And Analysis. An interactive open source software tool for a rapid first pass analysis. Available at https://foocheung.shinyapps.io/FFSv011/. Accessed on 01 July 2021.
67. Huynh-Thu VA, Irrthum A, Wehenkel L & Geurts P Inferring regulatory networks from expression data using tree-based methods. PLoS One 5(2010).
68. Bolger AM, Lohse M & Usadel B Trimmomatic: a flexible trimmer for Illumina sequence data. Bioinformatics 30, 2114–2120 (2014). [PubMed: 24695404]
69. Faust GG & Hall IM SAMBLASTER: fast duplicate marking and structural variant read extraction. Bioinformatics 30, 2503–2505 (2014). [PubMed: 24812344]
70. Dilthey AT, et al. HLA*LA-HLA typing from linearly projected graph alignments. Bioinformatics 35, 4394–4396 (2019). [PubMed: 30942877]
71. Snyder TM, et al. Magnitude and Dynamics of the T-Cell Response to SARS-CoV-2 Infection at Both Individual and Population Levels. medRxiv 2020.2007.2031.20165647 (2020).
72. ImmunoMind Team, Immunarch, R package version 0.5.5.; An R Package for Painless Bioinformatics Analysis of T-cell and B-cell Immune Repertoire Data. 2019. Available online: https://zenodo.org/record/3383240#.XoBv3i2B3jE.
73. Nolan S, et al. A large-scale database of T-cell receptor beta (TCRbeta) sequences and binding associations from natural and synthetic exposure to SARS-CoV-2. Res Sq (2020).
74. Blay N, et al. Assessment of kinship detection using RNA-seq data. Nucleic Acids Res 47, e136 (2019). [PubMed: 31501877]
75. Mulè MP, Martins AJ & Tsang JS Normalizing and denoising protein expression data from droplet-based single cell profiling. bioRxiv, 2020.2002.2024.963603 (2021).
76. McCarthy DJ, Chen Y & Smyth GK Differential expression analysis of multifactor RNA-Seq experiments with respect to biological variation. Nucleic Acids Res 40, 4288–4297 (2012). [PubMed: 22287627]
77. Law CW, Chen Y, Shi W & Smyth GK voom: Precision weights unlock linear model analysis tools for RNA-seq read counts. Genome Biol 15, R29 (2014). [PubMed: 24485249]
78. Love MI, Huber W & Anders S Moderated estimation of fold change and dispersion for RNA-seq data with DESeq2. Genome Biology 15, 550 (2014). [PubMed: 25516281]
79. Gupta NT, et al. Change-O: a toolkit for analyzing large-scale B cell immunoglobulin repertoire sequencing data. Bioinformatics 31, 3356–3358 (2015). [PubMed: 26069265]

Author Manuscript Author Manuscript Author Manuscript Author Manuscript

80. Mathew NR, et al. Single-cell BCR and transcriptome analysis after influenza infection reveals spatiotemporal dynamics of antigen-specific B cells. Cell Rep 35, 109286 (2021). [PubMed: 34161770]

81. Gadala-Maria D, Yaari G, Uduman M & Kleinstein SH Automated analysis of high-throughput B-cell sequencing data reveals a high frequency of novel immunoglobulin V gene segment alleles. Proc Natl Acad Sci U S A 112, E862–870 (2015). [PubMed: 25675496]

82. Gu Z, Eils R & Schlesner M Complex heatmaps reveal patterns and correlations in multidimensional genomic data. Bioinformatics 32, 2847–2849 (2016). [PubMed: 27207943]

83. Ding L, et al. Determination of human anticytokine autoantibody profiles using a particle-based approach. J Clin Immunol 32, 238–245 (2012). [PubMed: 22170314]

Author Manuscript Author Manuscript Author Manuscript Author Manuscript

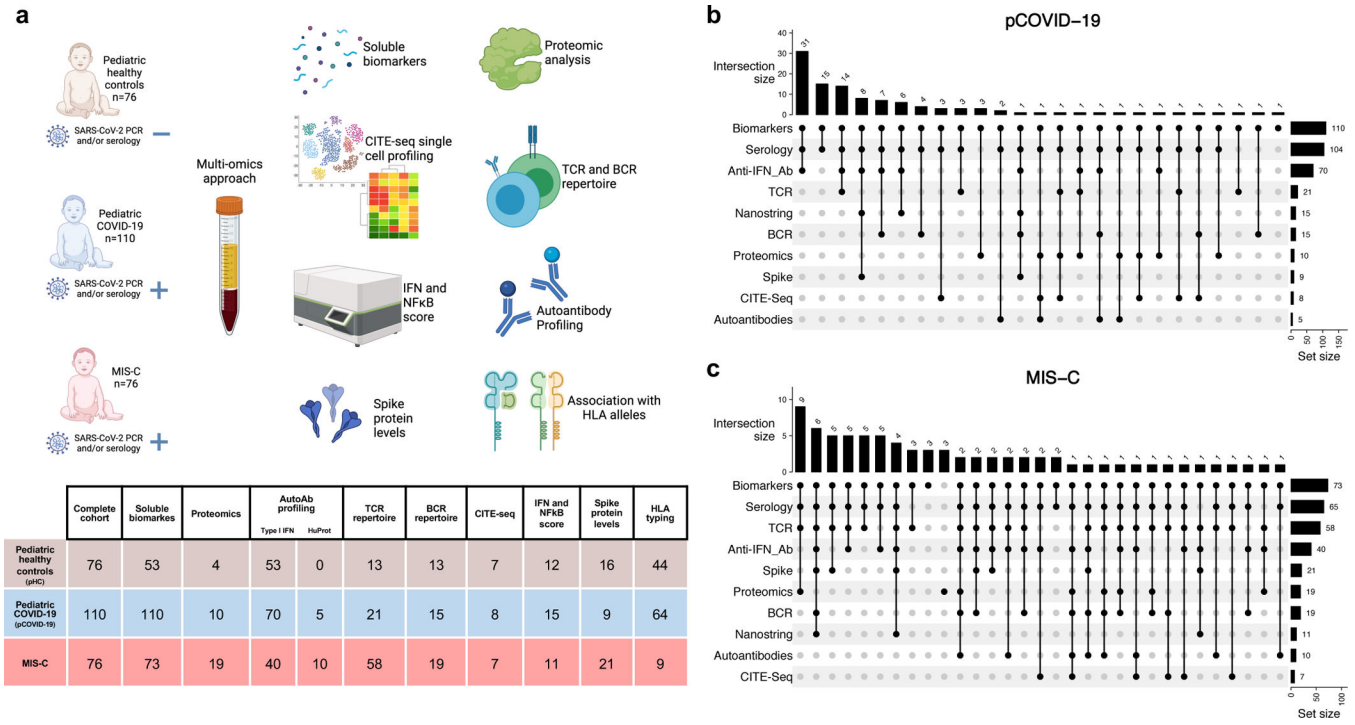

	Complete cohort	Soluble biomarkes	Proteomics	AutoAb profiling		TCR repertoire	BCR repertoire	CITE-seq	IFN and NFkB score	Spike protein levels	HLA typing
				Type I IFN	HuProt						
Pediatric healthy controls (pHC)	76	53	4	53	0	13	13	7	12	16	44
Pediatric COVID-19 (pCOVID-19)	110	110	10	70	5	21	15	8	15	9	64
MIS-C	76	73	19	40	10	58	19	7	11	21	9

Figure 1 - Study cohort and outline of the multi-omics approach.

a, Schematic representation of subject cohorts and workflow, with the number of subjects included in each analysis shown in the table. Figure created with BioRender.com.

b-c, The number of patients with pCOVID-19 (panel **b**) and MIS-C (panel **c**) analyzed by various combination of assays is shown by vertical bars on the top of the diagrams. The total number of patients analyzed with each assay is indicated by horizontal bars on the right of each panel.

Author Manuscript Author Manuscript Author Manuscript Author Manuscript

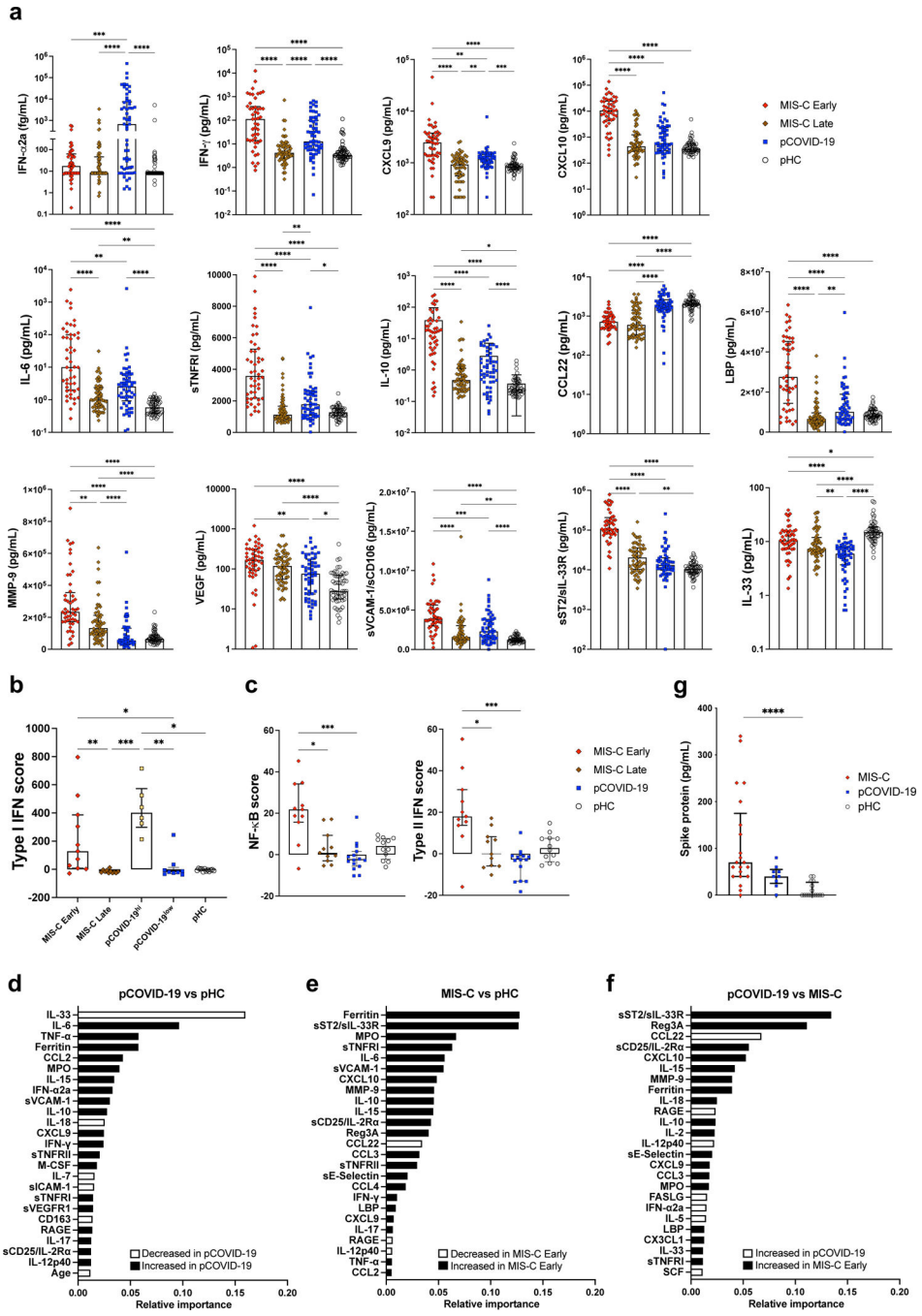

Figure 2 - Blood biomarkers analysis in pCOVID-19 and MIS-C.

a, Comparison of serum biomarker levels in children with multi-system inflammatory syndrome in children (MIS-C Early, n=48) (within 7 days since admission) and MIS-C Late (>7days, n=60), pediatric COVID-19 (pCOVID-19, n=57) within 7 days from symptom onset, and pediatric healthy controls (pHC, n=53).

b, Comparison of type I interferon (IFN) score in paired MIS-C Early and MIS-C Late (n=11), pHC (n=12), pCOVID-19 (n=15) with elevated (pCOVID-19^{hi}, n=6) and lower (pCOVID-19^{low}, n=9) IFN-α2a levels.

Author Manuscript Author Manuscript Author Manuscript Author Manuscript

c, Comparison of NF-κB score and type II IFN score in paired MIS-C Early and MIS-C Late (n=11), pCOVID-19 (n=15), and pHC (n=12).
d, Random forest classification comparing pCOVID-19 within 7 days from symptom onset (n=57) to pHC (n=53).
e, Random forest classification comparing MIS-C Early (n=48) to pHC (n=53).
f, Random forest classification comparing MIS-C Early (n=48) to pCOVID-19 within 7 days from symptom onset (n=57).
g, Serum Spike protein levels in MIS-C (n=21), pCOVID-19 (n=9) and pHC (n=16).
Maxima of box plots in panels **a**, **b**, **c** and **g** represent median values, and bars represent interquartile range. Statistical analysis in panels **a-c** and **g** was performed by Kruskal-Wallis test with adjustment for multiple comparisons. P values are marked as follows: * <0.05, ** <0.01, *** <0.001, and **** <0.0001.

Author Manuscript Author Manuscript Author Manuscript Author Manuscript

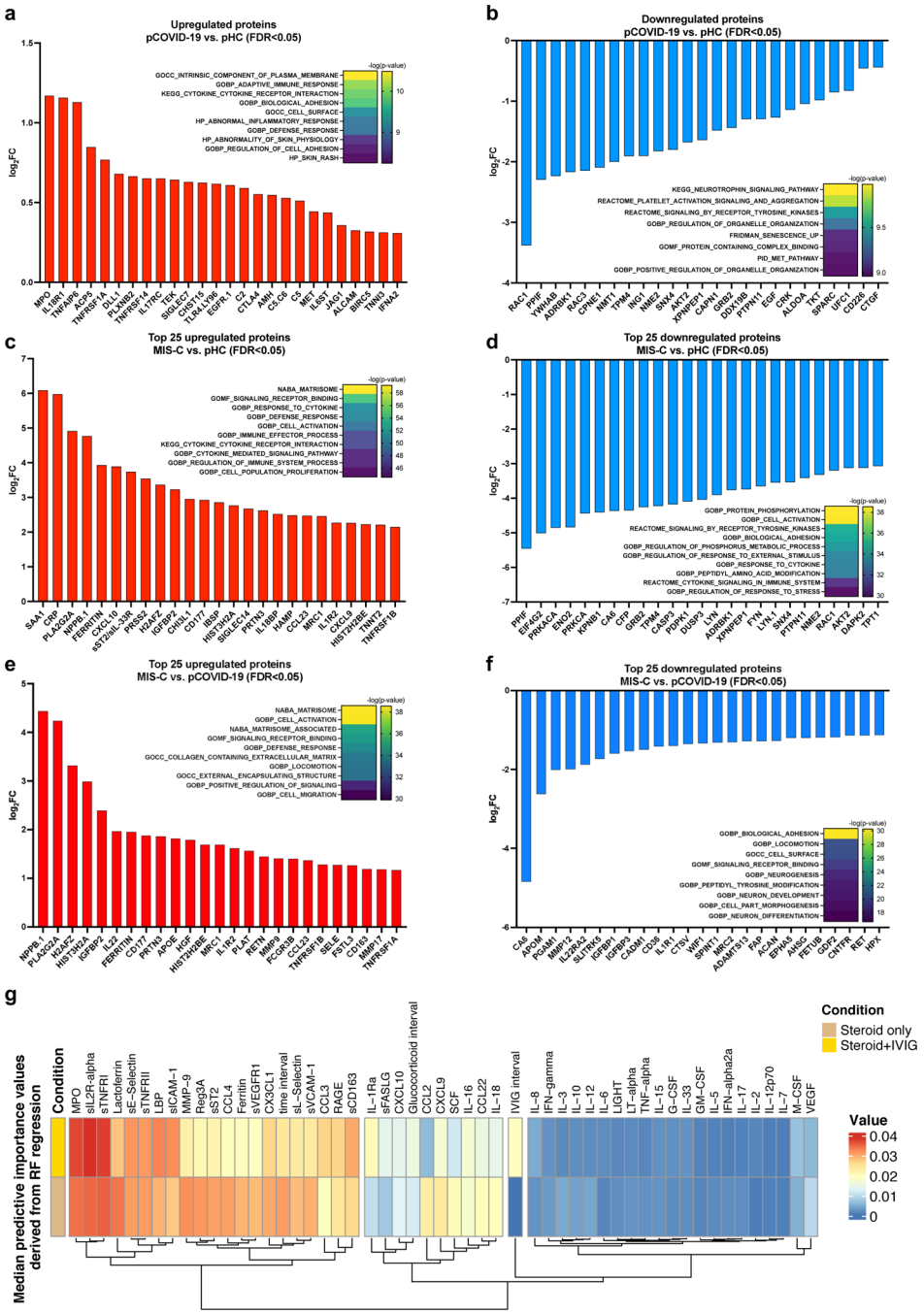

Figure 3 - Proteomic analysis in MIS-C compared to pCOVID-19.

a, b, Upregulated (panel **a**) and downregulated (panel **b**) plasma proteins obtained from the comparison between pCOVID-19 (n=10) and pHC (n=4).

c, d, Top 25 up- and down-regulated plasma proteins obtained from the comparison between MIS-C (within the first 7 days of hospitalization, n=16) and pHC (n=4).

e, f, Top 25 up- and down-regulated plasma proteins obtained from the comparison between MIS-C (within the first 7 days of hospitalization, n=16) and pCOVID-19 (n=10).

Author Manuscript Author Manuscript Author Manuscript Author Manuscript

g, Median predictive importance values derived from random forest regression of soluble biomarker values in a group of 101 samples obtained at various time points after hospitalization from 38 MIS-C patients who received both systemic glucocorticoids and IVIG, and in another group of 57 samples from 25 MIS-C patients who received systemic glucocorticoids only. In each random forest regression model (composed of 1000 decision trees with one model per target), predictive importance value for each predictor-target pair is computed using the algorithm described in ref.[66].

In panels **a-f**, top up- and down-regulated proteins were identified by selecting all proteins with false discovery rate (FDR) <0.05 and p value <0.05 (two-tailed *t*-test), and then ordering them according to increased or decreased fold-changes expressed in a log2 scale. Heatmaps show the most significantly enriched pathways for the group comparison and the statistical significance is expressed as -log(p value).

Author Manuscript Author Manuscript Author Manuscript Author Manuscript

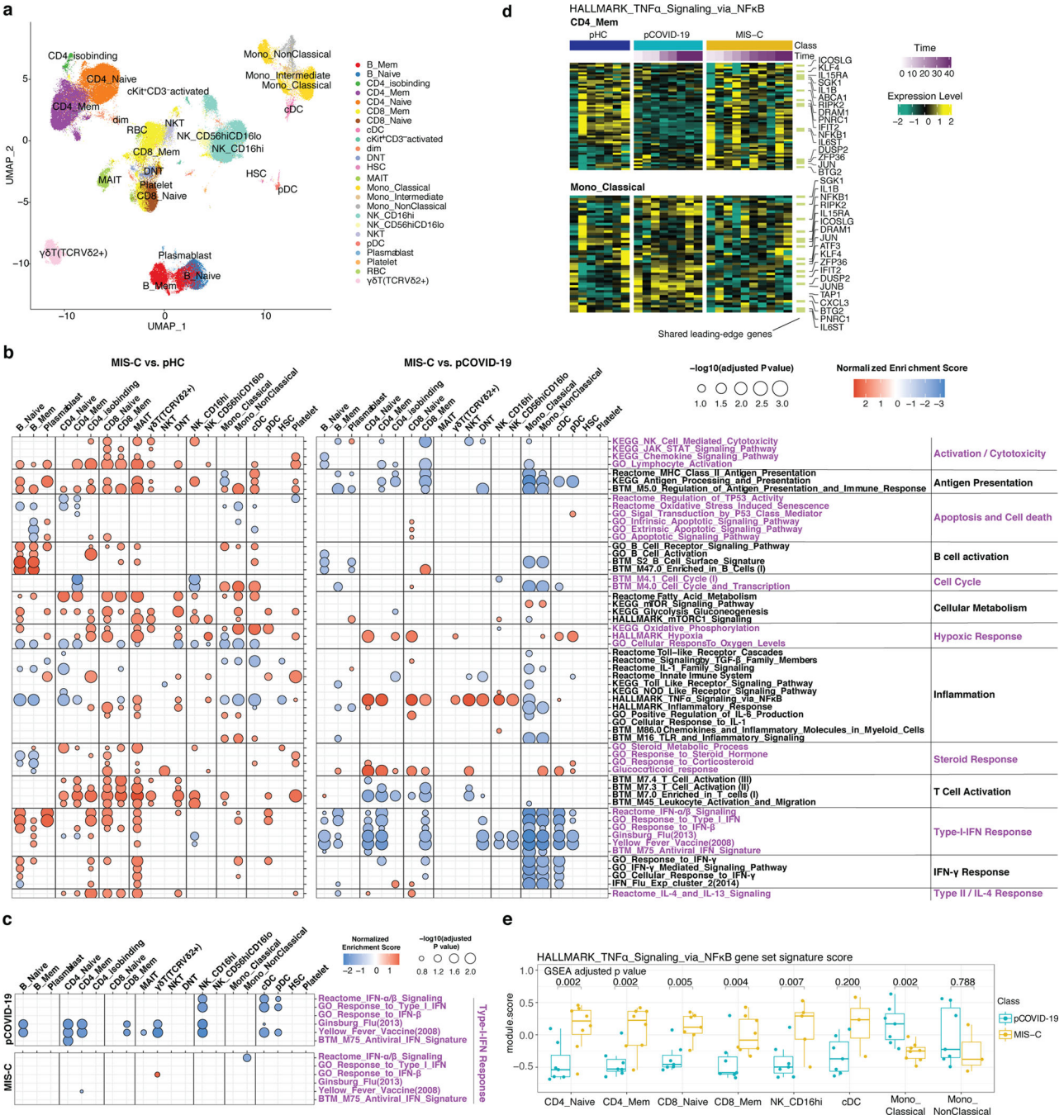

Figure 4 - Multimodal single cell profiling of MIS-C and pCOVID-19

a, UMAP visualization of single cell clusters based on protein expression profiles (see: Methods for cell type acronyms).

b, Gene set enrichment analysis (GSEA) of MIS-C *versus* pHC (left), and MIS-C *versus* pCOVID-19 (right), at timepoints within 40 days of admission. Selected gene sets are grouped into functional/pathway categories. Dot color denotes normalized gene set enrichment score and size indicates –log10(adjusted p value). P values were from GSEA test of the whole gene sets (see: Methods) and adjusted using the Benjamini-Hochberg method.

Author Manuscript Author Manuscript Author Manuscript Author Manuscript

The sample size for each group MIS-C n=8 (2 subjects with two timepoints), pCOVID-19 n=7, pHC n=7. Further details for statistical analysis are described in the Methods.

c, Gene set enrichment analysis (GSEA) result of pCOVID-19 (top) and MIS-C (bottom) based on the association with time (days since admission), only showing the type I IFN related response signatures. The sample size for each group MIS-C n=10 (3 subjects with two timepoints), pCOVID-19 n=8, pHC n=7.

d, Heatmap of HALLMARK_TNFa_Signaling_via_NFkB gene set in CD4+ Memory T cells and Classical Monocytes. Heatmap showing the scaled average mRNA expression (row z-score) of leading-edge (LE) genes from the GSEA analysis of MIS-C *versus* pCOVID-19. Shared LE genes and selected top LE from both cell types are labeled by gene symbol. The shared LE genes are annotated on the right column. Each column represents a sample. Subjects are grouped by pHC, pCOVID-19 and MIS-C classes, and columns are ordered by days since admission; also shown are the days since admission of each sample (top of the heatmaps).

e, Per-sample gene set signature scores of the HALLMARK_TNFα_Signaling_via_NFκB gene set in selected cell populations. Gene set scores were calculated using the gene set variation analysis of leading-edge genes from the MIS-C *versus* pCOVID-19 model (See Methods). P values shown are adjusted p values from GSEA result in (b). Box plot showing the median, first and third quantiles (lower and upper hinges) and smallest (lower hinge - 1.5*interquartile range) and largest values (upper hinge + 1.5* interquartile range) (lower and upper whiskers). Sample size was as follows: MIS-C, n=8 (2 subjects with two timepoints); pCOVID-19, n=7. See Methods for details of some low representative populations.

Author Manuscript Author Manuscript Author Manuscript Author Manuscript

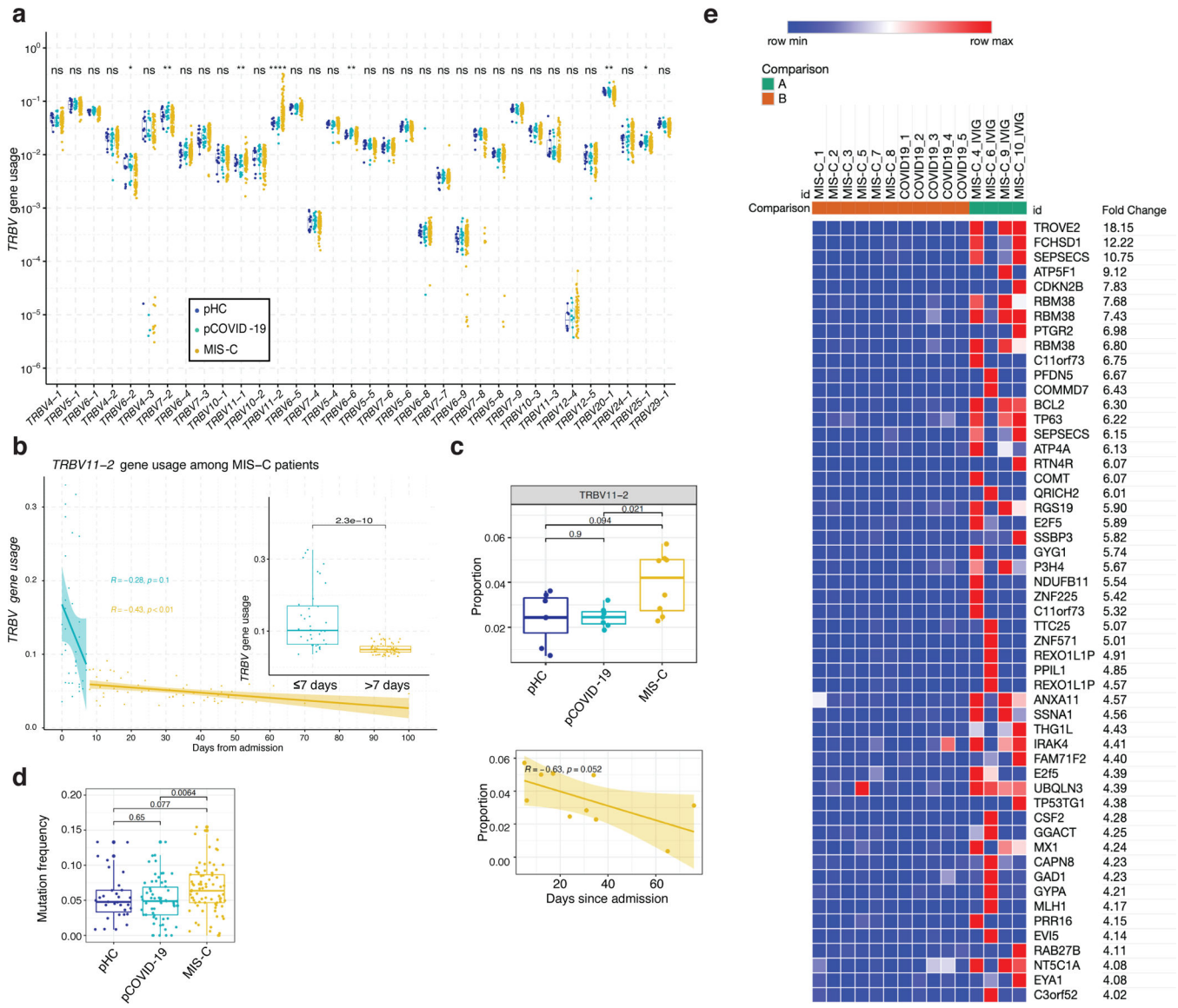

Figure 5 –. High-throughput sequencing and CITE-Seq analysis of T- and B-cell repertoire

a, *TRBV* gene usage in MIS-C (n=96 samples from 58 patients), pCOVID-19 (n=21 samples from 21 patients), and pHC (n=13 samples from 13 subjects). Clonotypes with ambiguous gene assignments are excluded from the figure. For each gene, non-parametric Kruskal-Wallis test with unadjusted P values was used to compare the three groups. ns: p > 0.05 (not significant), *: p<=0.05, **: p<=0.01, ***: p<=0.001, ****: p<=0.0001.

b, *TRBV11−2* gene usage observed in MIS−C patients within the first 7 days (in blue, n=36 samples from 35 patients) and at later time points (in yellow, n=59 samples from 44 patients) during hospitalization. Pearson correlation coefficient (number of days from admission *versus TRBV11−2* gene usage) and its p value are shown for both time intervals. The inset plot in the figure provides a comparison between the *TRBV11−2* gene usage distributions in these two-time intervals and a p value derived from two-tailed Wilcoxon rank sum test. Box plots show the median, first and third quantiles (lower and upper hinges)

Author Manuscript Author Manuscript Author Manuscript Author Manuscript

and smallest (lower hinge - 1.5*interquartile range) and largest values (upper hinge + 1.5* interquartile range) (lower and upper whiskers).

c, *Upper panel*: *TRBV11–2* usage (*TRBV11–2* ratio among each sample) in CD4+ T cells among three groups (pHC, n=7; pCOVID-19, n=7 and MIS-C, n=8 [2 subjects with two timepoints]) within 40 days of admission. P values shown are from two-sided Wilcoxon test between indicated two groups. ***Lower panel:*** *TRBV11–2* usage frequency in MIS-C CD4+ T cells over time (days since admission, n=10). Pearson correlation (R) and associated p values are shown. The shaded area represents standard error. Each dot indicates a sample. Box plot elements are the same as Figure 4e.

d, Mutation quantification of plasmablasts in the three groups (pHC, n=7; pCOVID-19, n=8 and MIS-C, n=7). P values shown were obtained using two-sided Wilcoxon test between indicated two groups. Each dot indicates a cell. Box plot elements are the same as Figure 4b.

e, Heatmap showing autoantibodies with the highest variance ordered by fold change, using a cut-off of four-fold change (see Methods). Comparisons were made between pCOVID-19 (n=5), MIS-C that did not receive IVIG (n=6), and MIS-C post-IVIG administration (MIS-C_IVIG, n=4).

Author Manuscript Author Manuscript Author Manuscript Author Manuscript

Table 1 -

Demographic, clinical and laboratory features

A. General description				
	pCOVID-19 (n=110)	MIS-C (n=76)[a]	pHC (n=76)	p value[b]
Sex (F/M)	41/69	35/41	31/29	0.168
Age, years – median (IQR)	5 (1–12)	8 (3–11)	8 (4–11)	0.033[c]
Ethnicity				
Caucasian	95/110 (86%)	36/76 (47%)	58/60 (96%)	<0.001
Hispanic/Latino	7/110 (6%)	35/76 (46%)	1/60 (2%)	<0.001
Black/African American	5/110 (5%)	5/76 (7%)	0	0.165
Asian	3/110 (3%)	0	1/60 (2%)	0.366
Comorbidities	46/110 (42%)	18/76 (24%)	19/60 (32%)[d]	0.034
Immunosuppressive therapy	2/110 (2%)	0	0	0.352
B. Clinical and laboratory data in pCOVID-19 and MIS-C patients				
	pCOVID-19 (n=110)	MIS-C (n=76)	p value	
Presenting signs and symptoms				
Fever	77/110 (70%)	76/76 (100%)	<0.001	
Upper respiratory (rhinorrhea, cough, sore throat/pharyngitis)	51/110 (46%)	12/76 (16%)	<0.001	
Pneumonia	17/110 (15%)	15/76 (20%)	0.425	
Dyspnea	10/110 (9%)	27/76 (36%)	<0.001	
Gastrointestinal (nausea, vomiting, diarrhea, abdominal pain)	32/110 (29%)	65/76 (86%)	<0.001	
Neurological (headache, irritability, drowsiness/somnolence, seizures)	22/110 (20%)	30/76 (39%)	0.115	
Rash	7/110 (6%)	47/76 (62%)	<0.001	
Cardiovascular	0	53/76 (70%)	<0.001	
Coronary artery involvement	0	4/53 (8%)	NA	
Cardiomyopathy/heart failure only	0	42/53 (79%)	NA	
Coronary artery involvement and cardiomyopathy/heart failure	0	7/53 (13%)	NA	
Shock	4/110 (4%)	36/76 (47%)	<0.001	
SARS-CoV-2 PCR positive[e]	99/110 (90%)	16/76 (21%)	<0.001	
SARS-CoV-2 serology positive	11/110 (10%)	76/76 (100%)	<0.001	
Laboratory anomalies				
ANC <1.0 x 10^9 cells/L	14/84 (17%)	0	<0.001	
ALC <1.5 x 10^9 cells/L	11/84 (13%)	46/71 (65%)	<0.001	
PLT <150 x 10^9/L	5/69 (7%)	31/71 (44%)	<0.001	
CRP >100 mg/L	2/76 (3%)	45/70 (64%)	<0.001	
Median CRP (IQR), mg/L	0.9 (0.3–7.4)	152 (54–264)	<0.001	
D-dimer >500 mg/L	34/59 (58%)	62/69 (90%)	<0.001	

Author Manuscript Author Manuscript Author Manuscript Author Manuscript

Ferritin >500 mg/L	3/28 (11%)	27/53 (51%)	<0.001
ALT >40 U/L	11/75 (15%)	34/69 (49%)	<0.001
C. Disease course in pCOVID-19 and MIS-C patients			
Asymptomatic	3/110 (3%)	0	NA
Mild	85/110 (77%)	0	NA
Moderate	17/110 (15%)	52/76 (68%)	NA
Severe	5/110 (5%)	24/76 (32%)	NA
D. Therapy in pCOVID-19 and MIS-C patients			
Gluococorticoids	9/110 (10%)	69/76 (91%)[f]	<0.001
IVIG	0	46/76 (61%)	<0.001
Biologics (in addition to glucocorticoids and/or IVIG)	0	12/76 (16%)	<0.001
Anakinra	0	7/12 (58%)	NA
Tocilizumab	0	3/12 (25%)	NA
Infliximab	0	2/12 (17%)	NA
Inotropes	0	21/76 (28%)	<0.001
Respiratory support	6/110 (5%)	28/76 (37%)	<0.001
Non-invasive	4/6 (67%)	16/28 (57%)	0.185
Mechanical ventilation	2/6 (33%)	12/28 (43%)	0.185

[a] Data in the table are reported for 60 pHC for whom detailed demographic, clinical and laboratory data were available

[b] Chi-square test except for age (Kruskal-Wallis test) and median CRP comparison (two-tailed Mann-Whitney U test)

[c] Kruskal-Wallis test; pairwise comparison was significant only between pCOVID-19 and pHC

[d] Control subjects had allergy as the only comorbidity

[e] pCOVID-19 patients negative for PCR had either positive immunoglobulin M or G for SARS-CoV-2. For MIS-C, patients had positive PCR within one week of admission.

[f] 42 of these received both glucocorticoids and IVIG

ALC, absolute lymphocyte count; ALT, alanine aminotransferase; ANC, absolute neutrophil count; CRP, C-reactive protein; F, female; IQR, interquartile range; IVIG, intravenous immunoglobulin; M, male; MIS-C, multisystem inflammatory syndrome in children; NA, not applicable; PCR, polymerase chain reaction; pCOVID-19, pediatric COVID-19; pHC, pediatric healthy controls; PLT, absolute platelet count; SARS-CoV-2, severe acute respiratory syndrome coronavirus 2.